Graphical Abstract

Synthesis

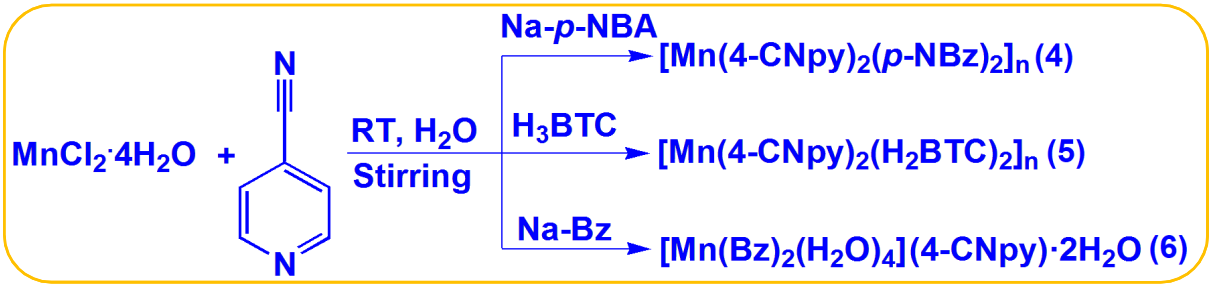

Molecular Structures

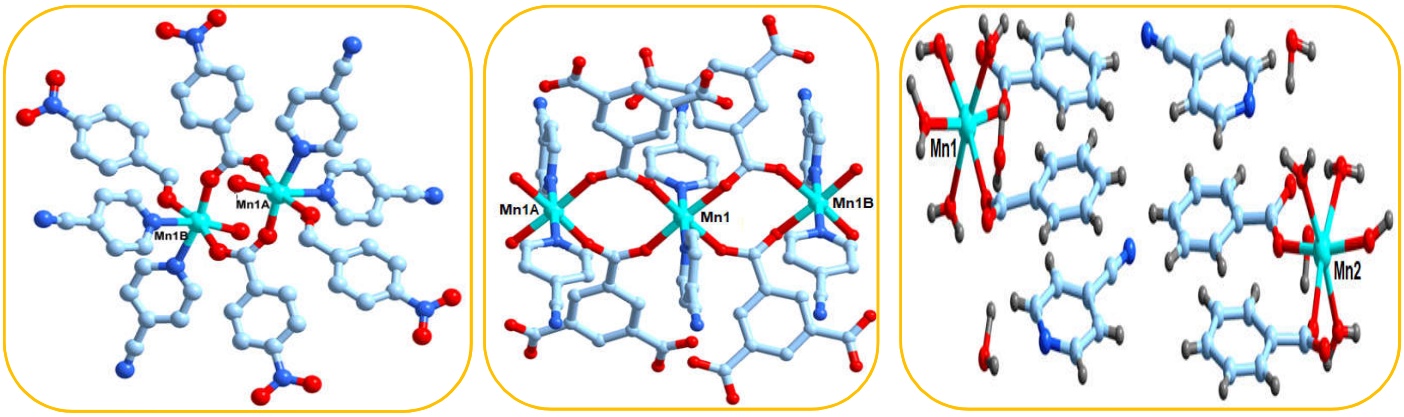

4 5 6

Self-Assembly

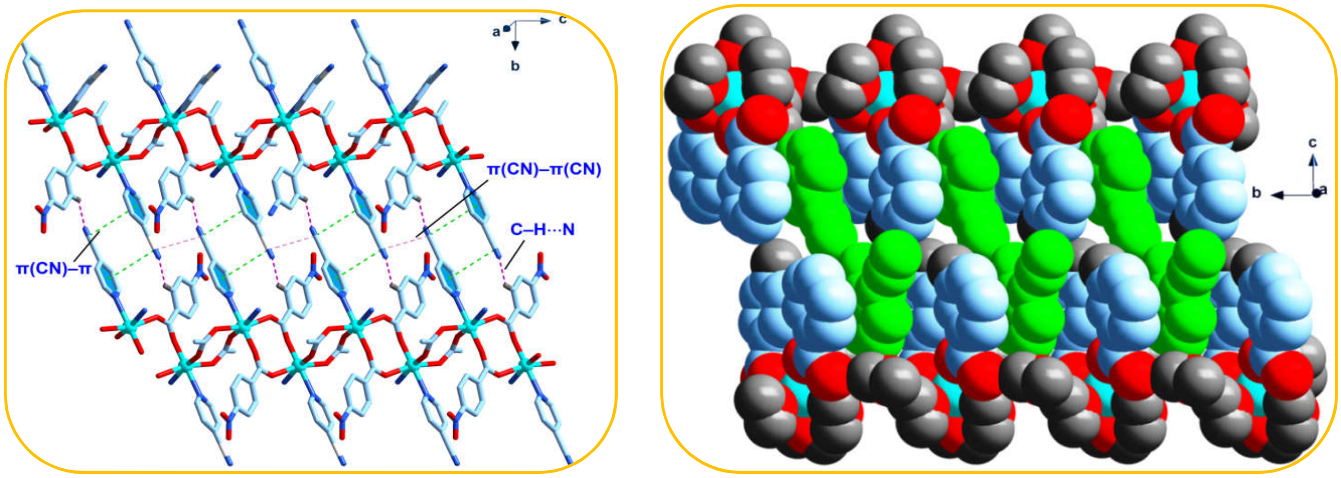

Theoretical Studies

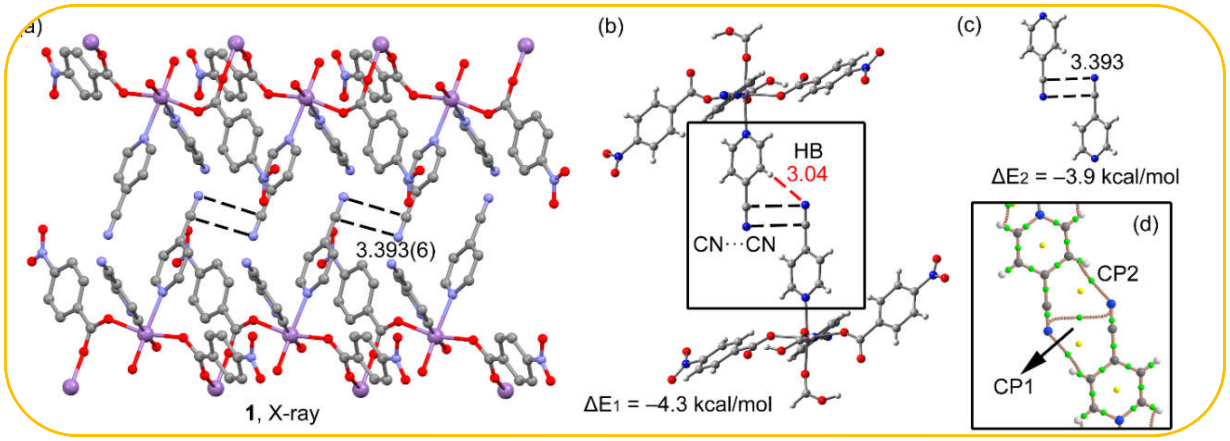

Chapter 3

Coordination Polymers and Unusual Werner Type Clathrate of Mn(II) involving Energetically Significant Nitrile-Nitrile and C–H···C Contacts: Synthesis, Supramolecular Assemblies and Theoretical Studies

3.1 INTRODUCTION

Crystal engineering involving supramolecular assemblies of coordination complexes or metal-organic hybrid materials has emerged as an important field in chemical research in recent years due to their potential applications in optical, electrical, magnetic and adsorptive materials.[1] The structural diversity of such promising compounds strongly depends on the chemical nature of the metal ions as well as primary or ancillary ligands.[2] Coordination polymers involving carboxylates have also gained much attention recently because of their ability to exhibit various dimensional networks with interesting properties.[3,4] O. Veselska *et al*. have recently reported copper(II) coordination polymers *viz*. $[Cu_2\{(O_2CPhS)_2\}_2(H_2O)_2]_n$ and $[Cu(p\text{-}SPhCO_2H)]_n$ involving substituted benzoic acid [where, $HSPhCO_2$ = 4-mercaptobenzoate and $(SPhCO_2)_2$ = 4,4′-dithiodibenzoate].[5] R. Miao and coworkers have developed three new solvent driven Zn(II) coordination polymers, *viz*. $\{[Zn(BTC)(NH_3)_2]\cdot 2H_2O\}_n$, $\{[Zn_3(BTC)_2(NH_3)_2(H_2O)_6]\cdot 2H_2O\}_n$ and $\{[Zn_3(BTC)_2(NH_3)_6]\cdot 5H_2O\}_n$ by using the same metal salt $[Zn(Ac)_2\cdot H_2O]$ and same ligand [1,3,5-benzenetricarboxylic acid (H_3BTC)] in different solvents.[6] Such structural diversity results from the fact that the carboxylate groups can bind metal centers in different ways (**Scheme 3.1**) and may account for the possible low dimensional materials to higher dimensional supramolecular frameworks.

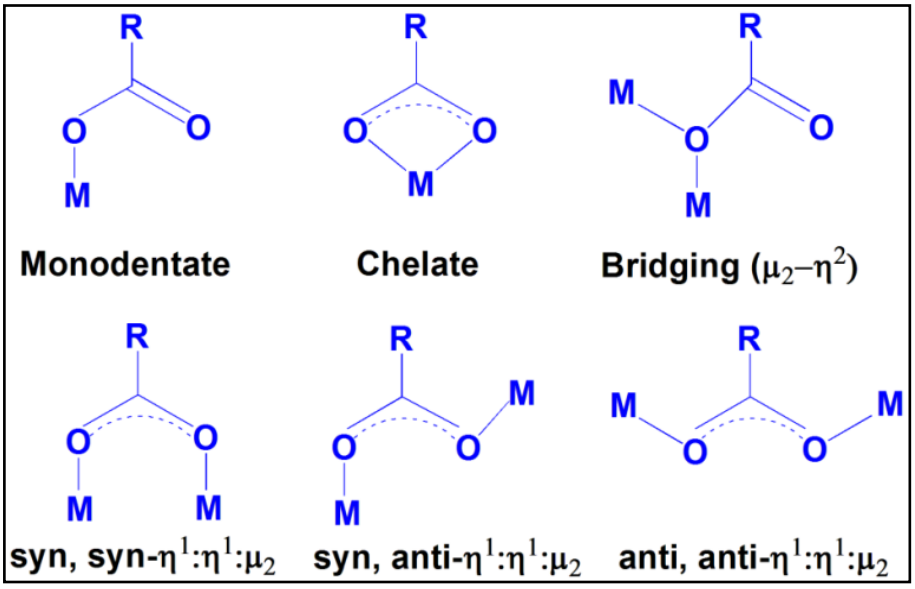

Scheme 3.1 Different coordination modes of the carboxylate moiety in coordination complexes.

Coordination bonds are stronger and have better directionality than other non-covalent interactions.[7] This makes the structural prediction of coordination compounds easier than molecular crystals. However, self assembly of systems consisting of metal ions, organic moieties, counter anions and solvent molecules with structural uncertainty is an intrinsic characteristic of such systems.[8] Weak non-covalent interactions such as hydrogen bonding, π–π stacking, C–H···π and anion-π interactions, which play a prominent role in sustaining supramolecular assemblies, have been widely explored in literature.[9] Besides these, other emerging non-covalent interactions *viz*. halogen bonding, π(chelate)···π, π(chelate)···π(chelate) etc. also play an important role in the formation of various interesting crystal structures.[10] In addition, two other non-conventional supramolecular interactions *viz*. C–H···C and nitrile-nitrile interactions also play pivotal roles in stabilizing interesting structures.[11] C–H···C contacts were identified much earlier[12], later studied theoretically[13] and established crystallographically.[14] This weak interaction arises due to the low acidity and basicity of the C–H and C moieties respectively. The interaction may be enhanced by the use of more acidic proton donor or by increasing the basicity of the acceptor.[15] These contacts are rather scarce in published literature.

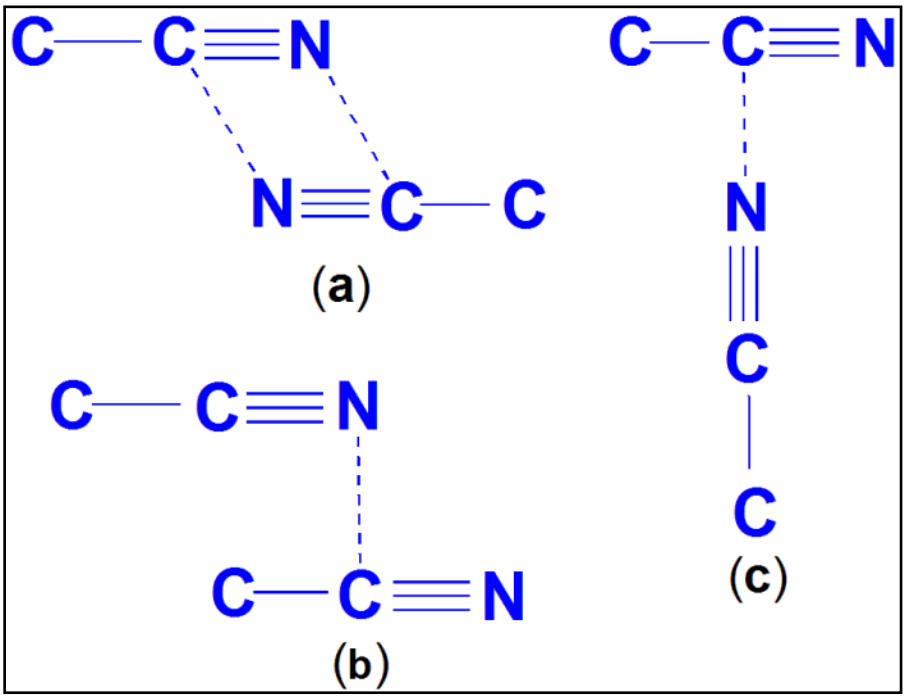

Scheme 3.2 Three different C≡N···C≡N interaction motifs: (**a**) sheared anti-parallel motif (**b**) sheared parallel motif and (**c**) perpendicular motif.

Supramolecular interactions involving the nitrile group are of particular interest as they exhibit local dipole moments which are similar to that of the carbonyl group.[16,17] As a polar functional group, nitrile group engages in dipole-dipole interactions and can serve as an H–bond acceptor, frequently participating in relatively weak and unconventional hydrogen bonding interactions.[18] As depicted in **Scheme 3.2**, three types of C≡N···C≡N interactions have been observed; (a) sheared anti-parallel motif, (b) sheared parallel motif and (c) perpendicular motif with anti-parallel motif the most dominant one, which involves symmetry-related pairs of C≡N groups.[19]

In metal-organic crystal engineering, clathrates are of particular interest because of their inclusion behaviour and use as catalysts, anti-oxidants and stabilizing agents.[20] As per IUPAC definition, they are inclusion compounds in which the guest atoms or molecules are constrained or trapped in the cages formed by the host molecule or by a lattice of host molecules via van der Waals or hydrogen bonding forces.[21] The clathrates find wide range of applications in many fields of chemistry, technological fields, material science and pharmaceutical industry in respect of numerous and diverse issues.[22] Although, inclusion behavior of organic compounds is well known[23], only a

few inorganic compounds *viz*. Hofmann and Werner type complexes exhibit such inclusion ability. Hofmann-type clathrates[24] have the general formula $ML_2M'(CN)_4 \cdot nG$, where M is a transition metal atom; M′ = Ni, Pd or Pt; L is either a bidentate or two monodentate ligand molecules, G is a guest molecule and n is the number of guest molecules, whereas Werner-type clathrates[25] may be represented by the general formula $MX_2A_4 \cdot 2G$; where M = Fe, Co, Ni, Cu, Zn, Cd, Mn or Hg, G = benzene, pyrrole, thiophene, dioxane, aniline or biphenyl, X = NCS^-, NCO^-, NO_3^-, NO_2^-, Cl^-, Br^- or I^- and A = pyridine and 4-methylpyridine. Merrill M. Wicht and his group have reported seven Ni(II) isothiocyanato Werner clathrates with seven polyaromatic hydrocarbons *viz*. indene, naphthalane, azulene, fluorene, anthracene, phenanthrene and pyrene.[26] F. J. Valverde-Muñoz *et al*. have also reported two 3D Hofmann-type Clathrates *viz*. [Fe(II)(pina)[M′$(CN)_2]_2$]·xMeOH (M′ = Ag, Au) [where, pina = N-(pyridin-4-yl)isonicotinamide].[27]

Design, synthesis and characterization of cocrystal hydrates have received remarkable attention as functional materials with potential applications in pharmaceutical[28] or electronic materials,[29] as well as in synthetic organic chemistry.[30] Cocrystal hydrates are very important from pharmaceutical point of view, which provide methods for developing new solid forms of active pharmaceutical ingredients[31] with tailored properties *viz*. enhanced dissolution rates, thermal stability or mechanical properties.[32,33] In that context, many research groups have recently developed various pharmaceutically active cocrystal hydrates.[34]

With an aim to explore the uncoventional supramolecular interactions in coordination solids, we, in this chapter, describe the syntheses and structural aspects of three Mn(II) complexes of the types $[Mn(4\text{-}NBz)_2(4\text{-}CNpy)_2]_n$ (**4**), $[Mn(4\text{-}CNpy)_2(H_2BTC)_2]_n$ (**5**) and $[Mn(Bz)_2(H_2O)_4]\cdot(4\text{-}CNpy)\cdot 2H_2O$ (**6**) [4-NBz = 4-nitrobenzoate, H_3BTC = 1,3,5-benzenetricarboxylic acid, 4-CNpy = 4-cyanopyridine, Bz = benzoate]. Crystal structure analyses reveal that compounds **4** and **5** are polymers involving 3D network structures that show anti-parallel nitrile···nitrile interactions, while compound **6** is an unusual Werner type clathrate involving energetically significant weak C–H···C contacts. The characteristics of anti-parallel nitrile···nitrile interactions in **4** and **5** were further studied theoretically using the quantum theory of atoms in molecules (QTAIM) and molecular electrostatic potential surface (MEPS). The

influence of the metal coordination on the strength of the nitrile···nitrile interaction was also studied. In compound **6**, the inclusion behavior involving the weak C–H···C contacts is analyzed by various theoretical techniques *viz*. QTAIM, Symmetry Adapted Perturbation Theory (SAPT) and non-covalent interaction (NCI) index analyses. These computational results suggest that the observed weak C–H···C interactions are energetically quite significant and both electrostatics as well as dispersion interactions are the most dominant contributors towards their stabilization.

3.2 EXPERIMENTAL

3.2.1 Materials and methods

All reagents *viz*. manganese(II) chloride tetrahydrate, 4-cyanopyridine, benzoic acid, benzene-1,3,5-tricarboxlic acid and 4-nitrobenzoic acid used in this work were obtained from commercial sources and used as received. De-ionized water was used as the reaction medium. Elemental (C, H and N) analyses were carried out using Perkin Elmer 2400 Series II CHNS/O analyzer. KBr phase FT-IR spectra were recorded in a Bruker APEX II FT-IR spectrophotometer in the mid-IR region (4000 to 500 cm^{-1}). Shimadzu UV-2600 spectrophotometer was used to record the diffuse-reflectance UV-Vis spectra. Thermogravimetric studies were carried out under the flow of N_2 gas using Mettler Toledo TGA/DSC1 STAR^e system at the heating rate of 10˚C min^{-1}. Room temperature magnetic susceptibility was measured at 300 K on a Sherwood Mark 1 Magnetic Susceptibility balance by Evans method.

3.2.2 Preparation of the complexes

3.2.2.1 Preparation of $[Mn(4\text{-}NBz)_2(4\text{-}CNpy)_2]_n$ (4)

Sodium salt of 4-nitrobenzoic acid (0.378 g, 2.0 mmol) was dissolved in 15 mL of distilled water in a round-bottom flask. An aqueous solution of $MnCl_2{\cdot}4H_2O$ (0.198 g, 1 mmol) was added to this solution. The solution was then stirred at room temperature for about an hour. To the resulting colorless solution, *4-CNpy* (0.208 g, 2 mmol) was added slowly and the mixture was stirred mechanically for about two hours (**Scheme 3.3**). The yellow product so obtained was then filtered and washed with de-ionised water. The filtrate was left unperturbed in cooling conditions for crystallization. Colorless crystals with irregular shape were obtained from the filtrate after few weeks with a yield of 74%

(yield = 0.440 g). The large crystals were filtered off, washed with water and dried in air. Anal. calcd. for $C_{26}H_{16}C_{l0}MnN_6O_8$ (Mw = 595.39): C, 49.50%; H, 2.56%; N, 13.32%. Found: C, 49.39%; H, 2.49%; N, 13.25%. IR (KBr pellet, cm^{-1}): 3414 (m), 3092 (sh), 2235 (m), 1942 (m), 1612 (vs), 1547 (m), 1496 (s), 1416 (vs), 1218 (s), 1115 (w), 1064 (m), 1005 (m), 831 (vs), 786 (m), 552 (m) [s, strong; m, medium; w, weak; br, broad; sh, shoulder]. μ_{eff} = 5.80 BM.

3.2.2.2 Preparation of [Mn(4-CNpy)$_2$(H$_2$BTC)$_2$]$_n$ (5)

A similar procedure to **4** was used for the synthesis of **5**, except that 1,3,5-benzene tricarboxylic acid (0.420 g, 2.0 mmol) was taken in place of sodium salt of 4-nitro benzoic acid (**Scheme 3.3**). Colorless crystals were obtained from the reaction mixture after two weeks with a yield of 79% (yield = 0.534 g). Anal. calcd. for $C_{30}H_{18}MnN_4O_{12}$ (Mw = 677.39): C, 52.88%; H, 2.66%; N, 8.22%. Found: C, 52.78%; H, 2.61%; N, 8.17%. IR (KBr pellet, cm^{-1}): 3429 (w), 3043 (sh), 2877 (w), 2243 (m), 1970 (w), 1609 (vs), 1577 (sh), 1536 (vs), 1457 (s), 1396 (s), 1350 (vs), 1210 (s), 1069 (s), 1010 (s), 917 (s), 836 (s), 783 (s), 723 (vs), 643 (sh), 536 (s) [s, strong; m, medium; w, weak; br, broad; sh, shoulder]. μ_{eff} = 5.84 BM.

3.2.2.3 Preparation of [Mn(Bz)$_2$(H$_2$O)$_4$](4-CNpy)·2H$_2$O (6)

Sodium salt of benzoic acid (0.288 g, 2.0 mmol) was added, under continuous stirring, to an aqueous solution (20 mL) of manganese(II) chloride tetrahydrate, $MnCl_2{\cdot}4H_2O$ (0.198 g, 1.0 mmol) and *4-CNpy* (0.104 g, 1.0 mmol) (**Scheme 3.3**). The stirring was continued for two hours at room temperature. The colourless product so obtained was filtered, washed with de-ionised water and kept in vacuum desiccator. The colorless solution obtained was then kept in a cooling condition for crystallization. After one week, colorless crystals of compound **6** suitable for single crystal XRD analysis were obtained with 84% yield (0.854 g). Anal. calcd. for $C_{40}H_{50}Mn_2N_4O_{20}$ (Mw = 1016.72): C, 47.25%; H, 4.96%; N, 5.51%. Found: C, 47.18%; H, 4.92%; N, 5.42%. IR spectral data (KBr disc, cm^{-1}): 3339(s), 3062(sh), 2968(sh), 2239(m), 1947(w), 1640(sh), 1597(s), 1546(sh), 1530(s), 1503(sh), 1415(sh), 1407(s), 1305(m), 1262(s), 1182(w), 1072(s), 1027(s), 933(w), 867(sh), 802(s), 706(s), 685(s), 568(s) [s, strong; m, medium; w, weak; br, broad; sh, shoulder]. μ_{eff} = 5.92 BM.

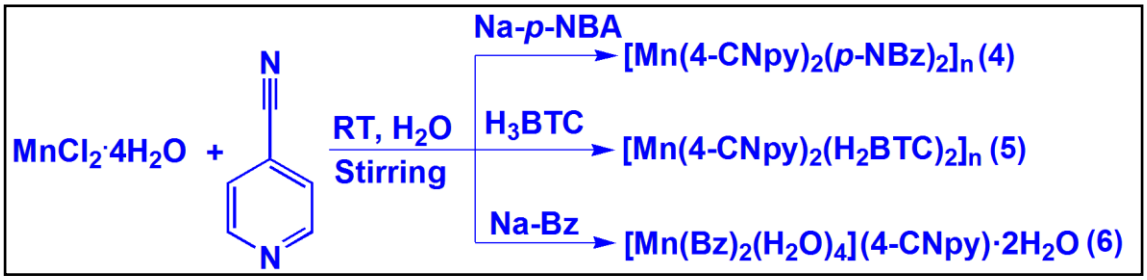

Scheme 3.3 Synthesis of compounds **4**, **5** and **6**.

3.2.3 X-ray crystallographic procedures

Crystal structures of **4**, **5** and **6** were determined by single crystal X-ray diffraction technique. X-ray diffraction data collection was carried out on a Bruker SMART CCD diffractometer with graphite monochromatized Mo Kα radiation (λ = 0.71073 Å). Semiempirical absorption correction, as well as scaling and merging the different datasets for each wavelength were performed with SADABS.[35] Crystal structures were solved and refined by the same techniques as discussed in Chapter 2. All non-hydrogen atoms were refined anisotropically. The hydrogen atoms in the crystal structures, except the lattice water molecules in **6**, were located from the difference Fourier maps and refined in the isotropic approximation. The hydrogen atoms of the lattice water molecules of **6** could not be located from the difference Fourier maps and are fixed at their normalized distances to obtain the hydrogen bonding patterns in the crystal structure. For complex **5**, the hydrogen atoms on the uncoordinated carboxylate groups of *H_3BTC* were not found and consideration of the hydrogen bonding interactions and C–O bond will depend on the localized positions of the hydrogen atoms. The structural diagrams were drawn with Diamond 3.2.[36] Data collection and refinement parameters for the complexes **4**, **5** and **6** are summarized in **Table 3.1**.

3.2.4 Theoretical methods

The calculations of the non-covalent interactions in the structures of the compounds **4** and **5** were computed using the Gaussian-09 program package.[37] We have used the M06-2X DFT method, because it is convenient for describing the weak non-covalent interactions properly, since it intrinsically takes into consideration the dispersion effects. Moreover, it is recommended for systems with transition metals[38] in

3.2.5 Crystal data

Table 3.1 Crystal and structure refinement data for **4**, **5** and **6**.

Parameters	**4**	**5**	**6**
Emprical formula	$C_{26}H_{16}MnN_6O_8$	$C_{30}H_{18}MnN_4O_{12}$	$C_{40}H_{50}Mn_2N_4O_{20}$
Formulae weight	595.39	677.39	1016.72
Temperature (K)	293(2)	296(2)	296(2)
Wavelength (Å)	0.71073	0.71073	0.71073
Crystal system	Monoclinic	Triclinic	Orthorhombic
Space group	*C*2/c	$P\bar{1}$	$Pca2_1$
a/Å	14.383(5)	10.068(5)	18.3680(9)
b/Å	26.102(5)	11.518(5)	7.4473(3)
c/Å	7.240(5)	13.991(5)	35.8518(17)
α^o	90.000(5)	67.891(5)	90
β^o	112.480(5)	75.807(5)	90
γ^o	90.000(5)	79.201(5)	90
Volume ($Å^3$)	2512(2)	1449.1(11)	4904.2(4)
Z	4	2	4
Calculated density (Mgm^{-3})	1.575	1.552	1.377
Absorption coefficient (mm^{-1})	0.590	0.530	0.592
F(000)	1212	686	2112
Crystal size (mm^3)	0.42 x 0.24 x 0.16	0.32 x 0.26 x 0.18	0.42 x 0.24 x 0.16
θ range for data collection (º)	1.14 to 25.00	1.60 to 26.25	1.14 to 25.00
Index ranges	–17<=h<=17, –31<=k<=32, –9<=l<=8	–12<=h<=11,–13<=k<=13, –17<=l<=14	–21<=h<=21, –8<=k<=8, –38<=l<=42
Reflections collected	9405	15727	54258
Refinement method	Full-matrix least-squares on F^2	Full-matrix least-squares on F^2	Full-matrix least-squares on F^2
Data / restraints / parameters	2588 / 0 / 186	5118 / 0 / 424	8141/1/597
Goodness-of-fit on F^2	1.063	1.061	1.094
Final *R* indices[$I>2\sigma(I)$] *R*1/ *wR*2	R1 = 0.0470, wR2 = 0.1422	R1 = 0.0464, wR2 = 0.1205	R1 = 0.0473, wR2 = 0.1215
R indices (all data) *R*1/ *wR*2	R1 = 0.1317, wR2 = 0.1761	R1 = 0.0684, wR2 = 0.1320	R1 = 0.0552, wR2 = 0.1324
Largest diff. peak and hole	0.700 and –1.060	0.348 and –0.461	1.491 and –0.514

$wR2 = \{\Sigma [w(F_o^2 - F_c^2)^2] / \Sigma [w(F_o^2)^2] \}^{1/2}$; $R1 = \Sigma | |F_o| - |F_c| | / \Sigma |F_o|$ *$GooF = S = \{\Sigma [w(F_o^2 - F_c^2)^2] / (n-p)^2$

order to describe correctly the CN···CN π-stacking interactions. The basis set used for the molecular electrostatic potential was 6-311+G* and the geometries were fullyoptimized. To evaluate the interactions in the solid state, we have used the crystallographic coordinates and the def2-TZVP basis set for all atoms. This procedure and level of theory have been successfully used to evaluate similar interactions.[39] The interaction energies were computed by calculating the difference between the energies of isolated monomers and their assembly. The interaction energies were calculated with correction for the basis set superposition error (BSSE) by using the Boys-Bernardi counterpoise technique.[40] The molecular electrostatic potential surfaces were computed using the Spartan software.[41] The Bader's theory of AIM[42] was computed at the same level M06-2X/def2-TZVP using the AIM all software.[43]

For complex **6**, the geometry of the supramolecular host tetramer of Mn(II) with the enclathrated *4-CNpy* molecules was fully optimized using the crystallographic coordinates with the global hybrid meta-GGA functional M06-2X.[44] We have used the relativistic small core effective core potential (ECP) of Stuttgart/Dresden (SDD)[45] for the transition metal and 6-31+G* basis set for the main group elements. Harmonic frequency calculations were performed at the same level of theory to characterize the nature of the stationary points. The structure was found to be local minimum and the optimized geometrical parameters were found to be very close to the structure obtained from single crystal XRD data. Quantum theory of atoms in molecules (QTAIM)[46] was performed at the same level of theory using Multiwfn suite of program.[47] Geometry optimization and frequency calculations were performed using Gaussian-16 suite of program.[48]

3.3 RESULTS AND DISCUSSION

3.3.1 Synthesis and general aspects

The complexes $[Mn(4\text{-}NBz)_2(4\text{-}CNpy)_2]_n$ (**4**), $[Mn(4\text{-}CNpy)_2(H_2BTC)_2]_n$ (**5**) and $[Mn(Bz)_2(H_2O)_4)](4\text{-}CNpy)\cdot 2H_2O$ (**6**) have been isolated in high yield by reacting one equivalent of $MnCl_2\cdot 4H_2O$ and two equivalents of *4-CNpy* with two equivalents of sodium salt of *4-NBz*, *H_3BTC* and two equivalents of sodium salt of *Bz* in water, respectively. Interestingly, the products obtained for compounds **4**, **5** and **6** during reaction resemble the single crystals obtained from the slow evaporation of the

respective mother liquors which has been confirmed by the FT-IR spectral studies. All the compounds are soluble in water as well as common organic solvents. Complexes **4**, **5** and **6** show room temperature (298 K) μ_{eff} values of 5.80, 5.84 and 5.92 BM respectively, which correspond to the high spin states for Mn(II) centers.[49]

3.3.2 Spectral properties

3.3.2.1 FT-IR Spectroscopy

FT-IR spectra of **4**, **5** and **6** (KBr pellets) were recorded in the region 4000-500 cm^{-1} (**Figure 3.1**). The strong peaks at around 1608 cm^{-1} for **4**, **5** and **6** indicate that the $–COO^-$ groups remain deprotonated upon coordination to the respective metal centers in them.[50] This is also corroborated by the absence of absorption bands in the range 1730-1680 cm^{-1}.[51] Similar deprotonation of carboxylate groups has been reported by Y. Xu *et al*. with the absence of absorption peaks at around 1700 cm^{-1} for two Cd(II) coordination polymers, $[Cd_2(CHDC)_2(APYZ)(H_2O)_2](H_2O)$ and $[Cd_2(CHDC)_2(PYZ)(H_2O)_2](H_2O)$ [where, H_2CHDC = 1,4- cyclohexanedicarboxylic acid, APYZ = 2-aminopyrazine, PYZ = pyrazine).[52] The peaks at (1565, 1379) cm^{-1} for **4** and (1496, 1368) cm^{-1} for **5** correspond to the asymmetric and symmetric vibrations of the carboxylate group ($–COO^-$), and the difference ($\Delta\nu$) is less than 200 cm^{-1}. For **6**, this difference is found to be 268 cm^{-1}. As discussed in the previous chapter, these observations indicate that the carboxylate groups in **4** and **5** coordinate to the metal ions in asymmetrical bridging mode (*syn*, *syn*-η^1:η^2:μ_2), whereas in **6**, it binds to the metal in a monodentate mode. M. Iqbal and coworkers have reported $\Delta\nu$ value of 258 for copper(II) complex having the formula [bipyCu(L)$_4$Cubipy] [where, bipy = 2,2′-bipyridine and L = 4-methoxy-2-phenyl acetate] to corroborate the monodentate coordination of carboxylate to Cu(II) centre.[53] The moderately strong vibrations at around 2241 cm^{-1} for **4**, **5** and **6** can be assigned to the nitrile stretching frequency ν(C≡N) of the *4-CNpy*. The positions of the ν(C≡N) bands in them remain almost unaffected from that of the free ligand, implying the *4-CNpy* is not coordinated to the metal through the nitrile group.[54] For **4**, the bands at 1555 and 1349 cm^{-1} are respectively assigned to the asymmetric and symmetric stretching vibration of the $–NO_2$ group[55], while the bands at 837 and 724 cm^{-1} for **5** are due to 1,3,5-tricarboxylatic acid.[56] Similar peaks at 752 and 731 cm^{-1} were reported by A. Tahli *et al*. for

asymmetric and symmetric stretching vibration 1,3,5-tricarboxylatic acid in a Cd(II) 1D polymer *viz*. $[Cd(H_2O)_6][Cd_2(atr)_2(\mu^2\text{-}BTC)_2(H_2O)_4]\cdot 2H_2O\}_n$.[57] A. Masoudiasl *et al*. have reported the asymmetric and symmetric stretching vibration of the $-NO_2$ group at 1521 and 1348 cm^{-1} respectively for a new nanostructured cadmium complex involving a tridentate schiff base ligand.[58]

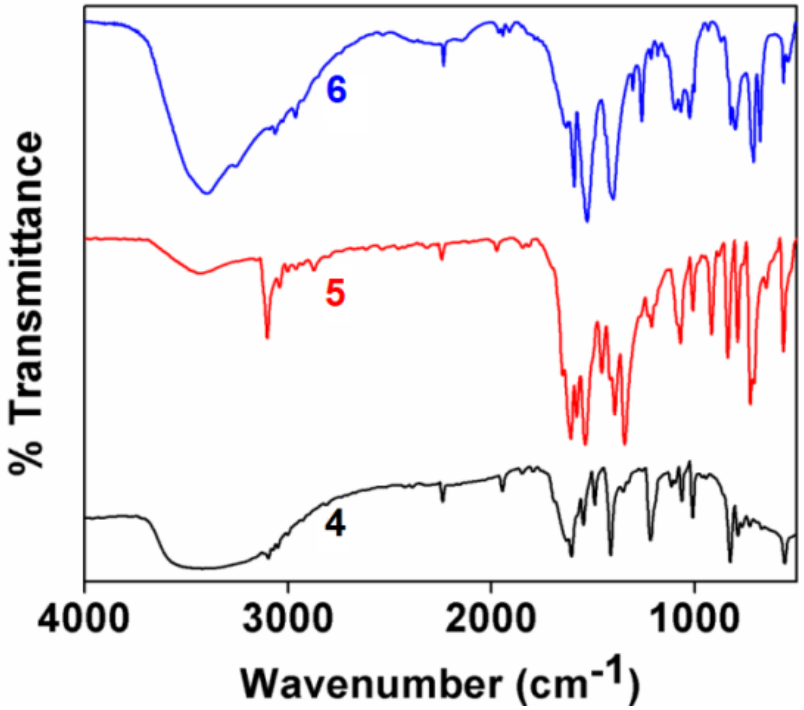

Figure 3.1 FT-IR spectra of **4**, **5** and **6**.

3.3.2.2 Electronic Spectroscopy

The electronic spectra of **4**, **5** and **6** were recorded in aqueous medium as well as in the solid state (**Figure 3.2**). As discussed earlier, the complexes do not show any d-d transition. The absorption at 219 nm, 221 nm and 230 nm for **4**, **5** and **6** respectively can be assigned to the $\pi\rightarrow\pi^*$ absorption of the ligands present whereas those around 276 nm, 240 nm and 270 nm can be attributed to the LMCT [O (or N) →Mn)] transitions respectively [**Figure 3.2(b)**].[59] In the solid state UV-Vis-NIR diffuse reflectance spectra [**Figure 3.2(a)**], however, the intra-ligand $\pi\rightarrow\pi^*$ absorption peaks for **4**, **5** and **6** are found to shift to 237 nm, 269 nm and 297 nm respectively. Because there are two species of direct coordinated atoms (O and N) with different electronegativities in **4** and

5, the LMCT absorption bands are split into two bands (327, 373 nm for **4** and 325, 368 nm for **5**) i.e. O→Mn and N→Mn respectively.[60] The same peak in **6** is found at 351 nm.

The differences in the ligand field bands of the three complexes in the two phases suggest that the bonding modes of the ligands as well as the geometry of the complexes undergo some structural distortion in the solution phase.[61] Y. Zheng *et al*. have also reported similar electronic spectra for benzoate based coordination compounds of Cu(II) viz. $[Cu_4(dmoxba)_2(bpy)_2(CH_3OH)_2](pic)_2\cdot 2H_2O$ and $[Cu_4(dmoxba)_2(phen)_2](pic)_2\cdot 2CH_3OH$ [where dmoxba, pic, bpy and phen stand for the anion of 2-{N-[2-(dimethylamino)ethyl]oxamido}benzoate, picrate, 2,2′-bipyridine and 1,10-phenanthroline, respectively].[62]

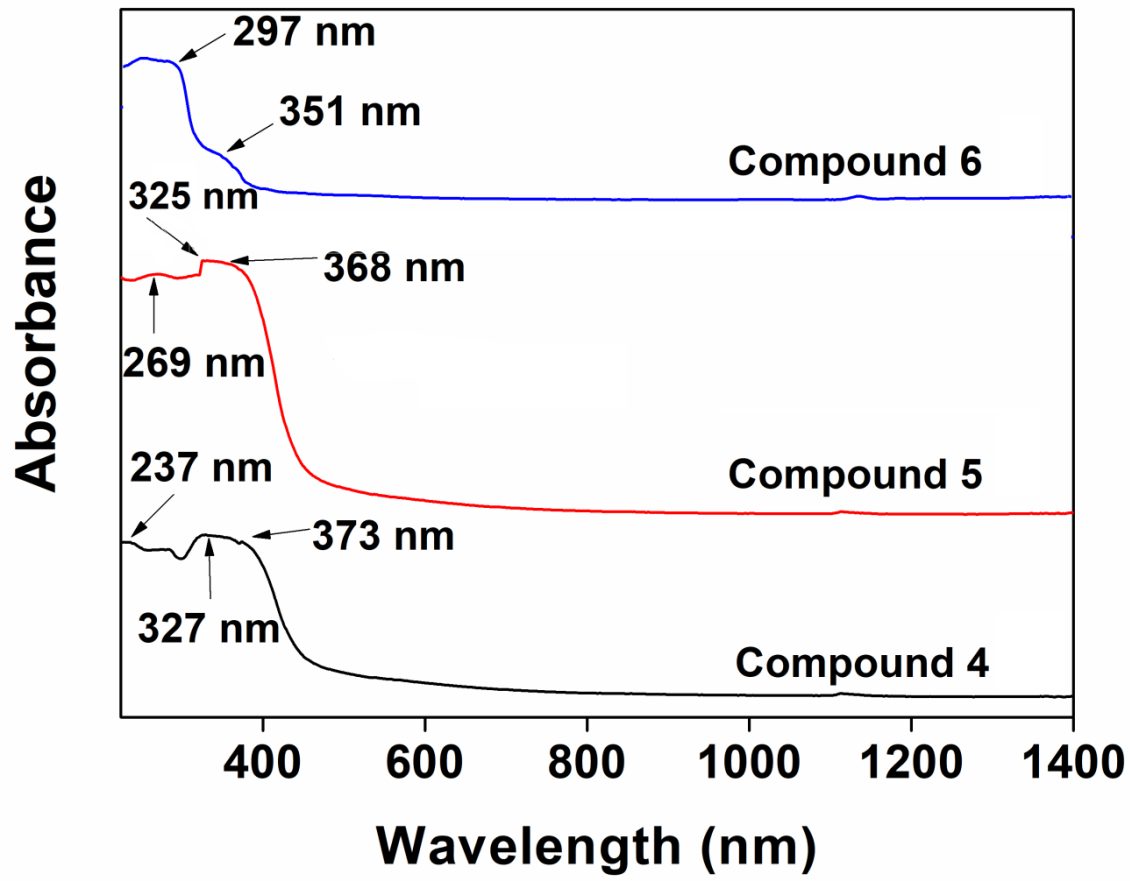

(**a**)

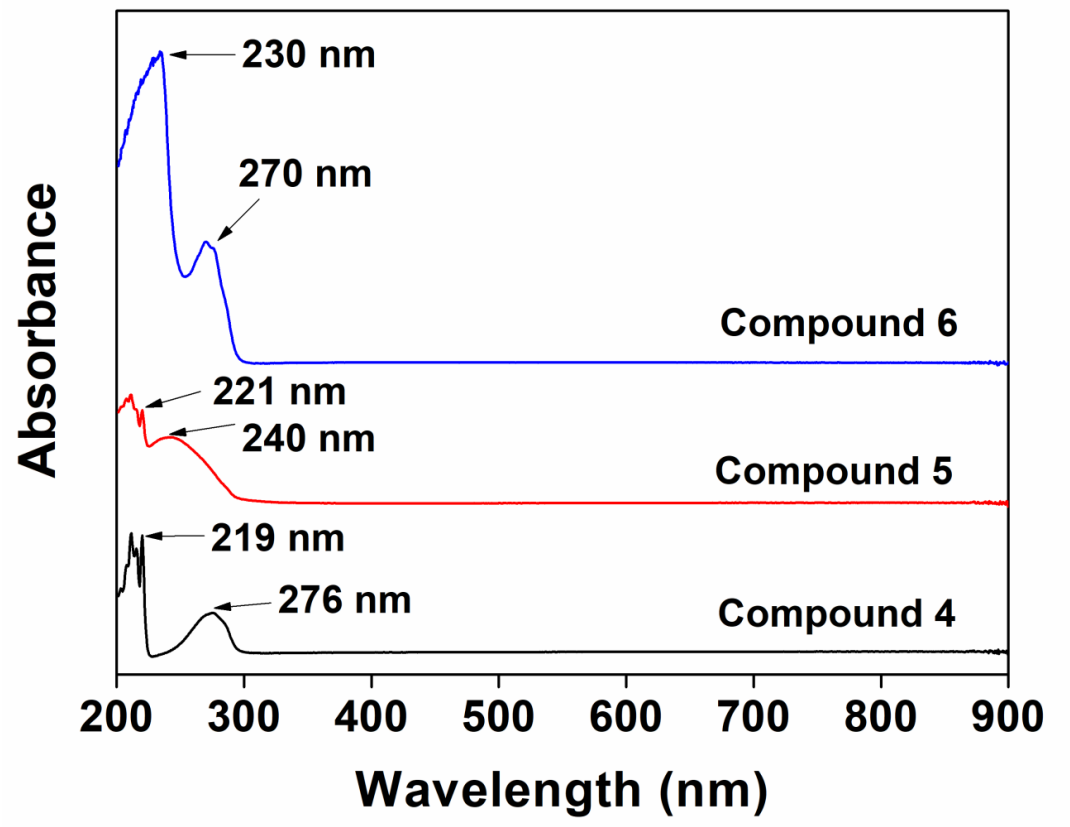

(**b**)

Figure 3.2(**a**) UV-Vis-NIR and (**b**) UV-Vis spectra of $[Mn(4\text{-}NBz)_2(4\text{-}CNpy)_2]_n$ (**4**), $[Mn(4\text{-}CNpy)_2(H_2BTC)_2]_n$ (**5**) and $[Mn(Bz)_2(H_2O)_4)](4\text{-}CNpy)\cdot 2H_2O$ (**6**) in solid and in aqueous phases.

3.3.3 Crystal structures

3.3.3.1 Crystal structure of $[Mn(4\text{-}NBz)_2(4\text{-}CNpy)_2]_n$ (4)

The details of single crystal XRD and structure refinement data of compounds **4**, **5** and **6** are presented in **Table 3.1**. Selected bond lengths and bond angles of compound **4** are summarized in **Table 3.2**. Compound **4** crystallizes in monoclinic crystal system with space group *C*2/c. The polymeric unit is shown in **Figure 3.3** together with the atom numbering scheme. The crystal structure of the polymer **4** contains a basic centro-symmetric dimeric unit $[Mn_2L_4L'_4]$ (where L = *4-CNpy* and L´ = *4-NBz*) in which the equatorial plane of both six coordinate Mn(II) ions is formed by the two *4-CNpy* and two oxygen atoms (O4A, O4D for Mn1A and O4B, O4C for Mn1B) (A. x, y, –1+z; B. –x, 2–y, 1 – z; C. x, 2–y, –0.5 + z; D. –x, y, 0.5–z) from two different bridging *4-NBz*.

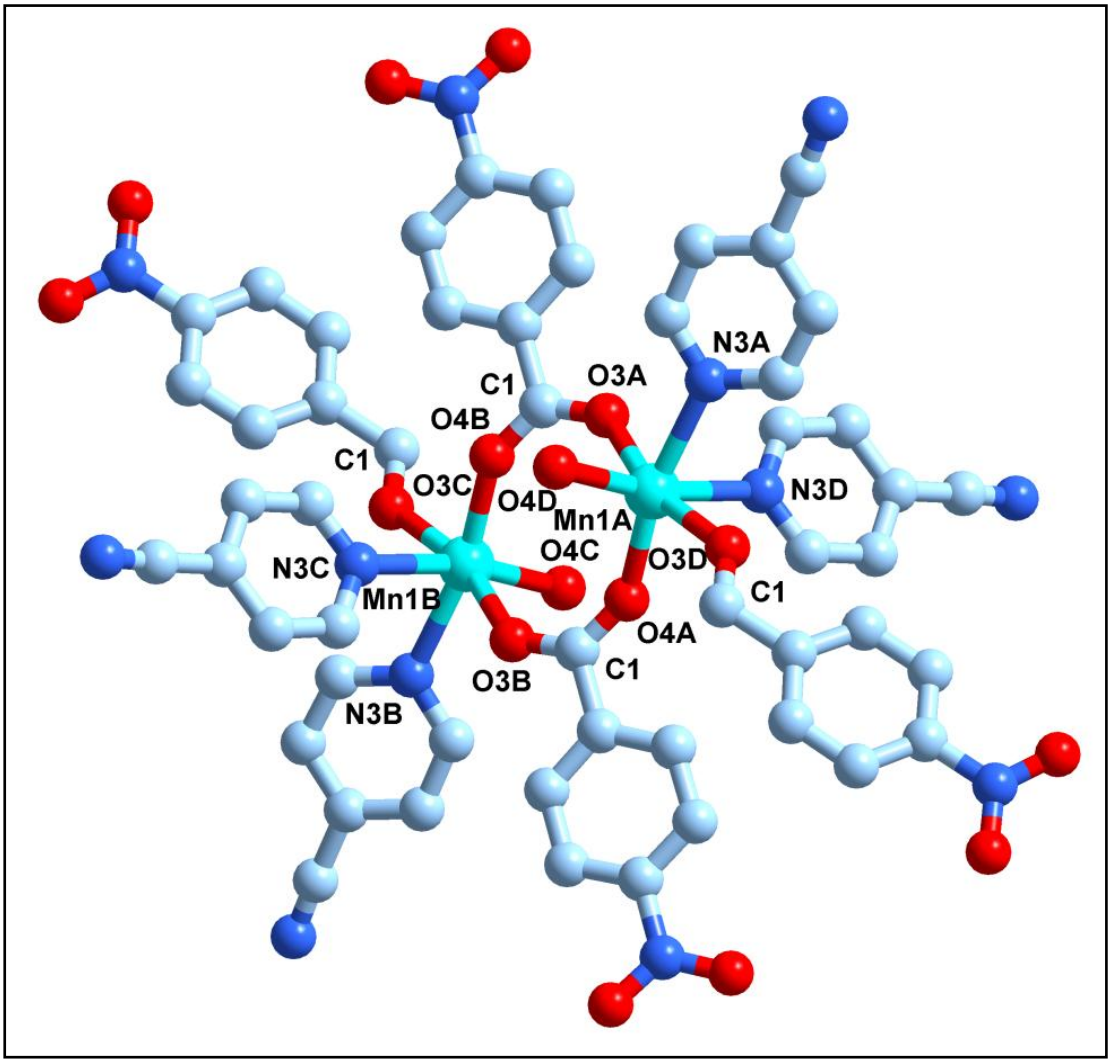

Figure 3.3 View of the coordination environment of Mn(II) in $[Mn(4\text{-}NBz)_2(4\text{-}CNpy)_2]_n$ (**4**). All hydrogen atoms are omitted for clarity. Symmetry codes: A. x, y, –1+z; B.–x, 2–y, 1–z; C. x, 2–y, –0.5+z; D.– x, y, 0.5–z.

The distorted octahedral coordination sphere around each Mn(II) ion in the polymer is completed by two trans axial oxygen atoms (O3A, O3D) for Mn1A and O3B, O3C for Mn1B) from other two different bridging *4-NBz*. The Mn–O bond distances to the bridging carboxylates [2.164(8) and 2.107(5) Å] are shorter than the Mn–N bond distances [2.340(5) Å] to the coordinated *cis 4-CNpy* molecules. P. Kar *et al.* also have reported the crystal structure of a Mn(II) polymeric complex, [Mn(4,4´-azpy)(4-$(NO_2)C_6H_4COO)_2$] (4,4´-azpy = 4,4´-azobis(pyridine)] with similar bridged *4-*

NBz ligands.[40] The Mn–O and Mn–N bond distances of this complex are comparable with those of compound **4**. The Mn···Mn distance of the dimeric unit of the polymer is 4.647(2) Å. R. Ye and his group have reported a Mn(II) coordination polymer $[Mn_3(IDPA)_3(DMA)(H_2O)_2]_n \cdot n[(H_2O)(DMA)]$ [where, H_2IDPA = 5-(1-oxoisoindolin-2-yl) isophthalic acid, DMA = N,N-dimethylacetamide] with Mn···Mn distances (Mn1···Mn2, Mn2···Mn3 and Mn1···Mn3) of 3.7202(6), 3.6661(6), 7.0658(6) Å, respectively.[64] The four atoms in the equatorial plane of each Mn centre in compound **4** are almost coplanar with a r.m.s. deviation of 0.0071 Å. The bridging mode of the carboxylate group linking the Mn1A atom (x, y,–1+z) to its centro-symmetrically related Mn1B atom (–x, 2–y, 1–z) to make the dinuclear $[Mn_2(4\text{-}NBz)_4(4\text{-}CNpy)_4]$ core is *syn-syn* with torsion angles of 51.0(61)° (O3A−C1−O4B−Mn1A) and 32.4(51)° (O4A−C1−O3B−Mn1B).

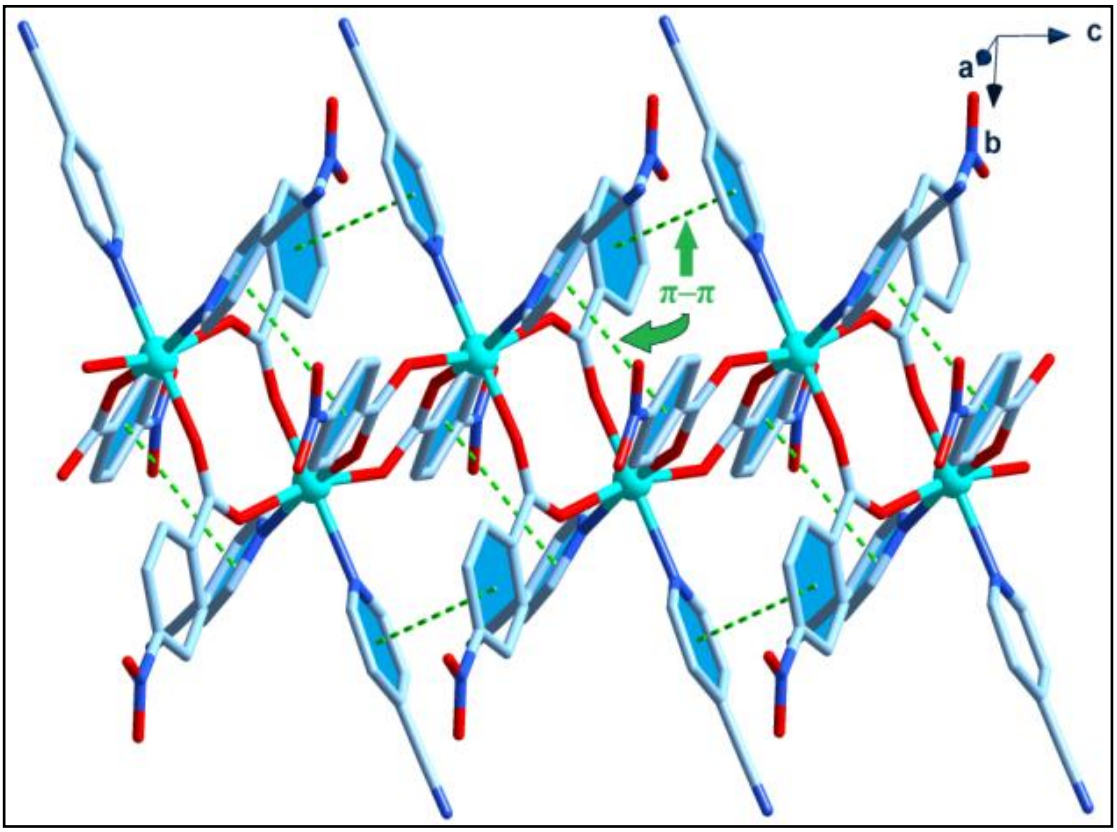

Figure 3.4 Polymeric 1D double-chain of $[Mn(4\text{-}NBz)_2(4\text{-}CNpy)_2]_n$ (**4**) featuring adjacent dinuclear units $[Mn_2(CO_2)_4N_4]$ along the *c*-direction. All hydrogen atoms are omitted for clarity.

Table 3.2 Selected bond lengths and angles (Å and °) for compound **4**.

Bond	d, Å	Angle	Degree (°)
Mn(1A)–O(3A)	2.164(8)	O(3A)–Mn(1A)–N(3A)	84.3(1)
Mn(1A)–O(3D)	2.164(8)	O(3A)–Mn(1A)–N(3D)	83.5(9)
Mn(1A)–O(4A)	2.107(5)	O(3A)–Mn(1A)–O(3D)	163.6(1)
Mn(1A)–O(4D)	2.107(5)	O(3A)–Mn(1A)–O(4A)	101.5(1)
Mn(1A)–N(3A)	2.340(5)	O(3A)–Mn(1A)–O(4D)	88.7(1)
Mn(1A)–N(3D)	2.340(5)	N(3A)–Mn(1A)–N(3D)	83.4(1)
		N(3A)–Mn(1A)–O(3D)	83.5(9)
		N(3A)–Mn(1A)–O(4A)	168.1(9)
		N(3A)–Mn(1A)–O(4D)	86.9(7)
		N(3D)–Mn(1A)–O(3D)	84.3(1)
		N(3D)–Mn(1A)–O(4A)	86.9(7)
		N(3D)–Mn(1A)–O(4D)	168.1(9)
		O(3D)–Mn(1A)–O(4A)	88.7(1)
		O(3D)–Mn(1A)–O(4D)	101.5(1)
		O(4A)–Mn(1A)–O(4D)	103.4(1)
Mn(1B)–O(3B)	2.164(8)	O(3C)–Mn(1B)–O(4B)	88.7(1)
Mn(1B)–O(3C)	2.164(8)	O(3C)–Mn(1B)–O(4C)	101.5(1)
Mn(1B)–O(4B)	2.107(5)	O(3C)–Mn(1B)–O(3B)	163.6(2)
Mn(1B)–O(4C)	2.107(5)	O(3C)–Mn(1B)–N(3B)	83.5(9)
Mn(1B)–N(3B)	2.340(5)	O(3C)–Mn(1B)–N(3C)	84.2(1)
Mn(1B)–N(3C)	2.340(5)	O(4B)–Mn(1B)–O(4C)	103.4(1)
		O(4B)–Mn(1B)–O(3B)	101.5(1)
		O(4B)–Mn(1B)–N(3B)	168.1(9)
		O(4B)–Mn(1B)–N(3C)	86.9(7)
		O(4C)–Mn(1B)–O(3B)	88.7(1)
		O(4C)–Mn(1B)–N(3B)	86.9(7)
		O(4C)–Mn(1B)–N(3C)	168.1(9)
		O(3B)–Mn(1B)–N(3B)	84.3(1)
		O(3B)–Mn(1B)–N(3C)	83.5(9)
		N(3B)–Mn(1B)–N(3C)	83.4(1)

The linking of the adjacent dinuclear cores in the polymer **4** by two of the bridging *4-NBz* forms a polymeric 1D double-chain structure that extends along the crystallographic *c*-direction (**Figure 3.4**). Within the polymeric chain, aromatic π–π stacking interactions are observed between the adjacent dimeric units, with both the *4-CNpy* and *4-NBz* moieties attached to the Mn(II) centers involved in π-π stacking with centroid-centroid separation of 3.883 Å. B. R. Srinivasan and G. K. Rane have also reported similar π–π stacking involving *4-NBz* moieties with centroid-centroid separation of 3.850 Å in $[Ni(H_2O)_4(\eta^1\text{-}4\text{-}NBz)_2]\cdot 2H_2O$ (*4-NBz* = 4-nitrobenzoate).[65] The 1D double-chains of **4** are connected in two ways. Along the *ac* plane, they are connected through the NO_2 group of *4-NBz* in a layered architecture [**Figure 3.5**(**a**)]. A seven-member supramolecular ring motif, expressed as $R_2^2(7)$ in the graph-set notation

of Etter is formed by the cooperative interaction between the $–NO_2$ group of *4-NBz* in one chain and the H8 and H9 atoms of the pyridine ring of *4-CNpy* in an adjacent chain. The hydrogen and the oxygen atoms are connected by weak supramolecular C8–H8···O2 and C9–H9···O1 interactions with C–H···O distances of 2.798 and 2.608 Å respectively in the layered supramolecular arrangement in the *ac* plane (**Table 3.5**). Similar weak supramolecular C–H···O interactions involving *4-NBz* have been reported by B. R Srinivasan *et al*. for $[Co(H_2O)_2(DMSO)_2(4\text{-NBz})]4\text{-NBz}$ (DMSO = dimethylsulfoxide; *4-NBz* = 4-nitrobenzoate).[66] The shortest inter-chain Mn···Mn distance in compound **4** along this direction is 13.40(44) Å.

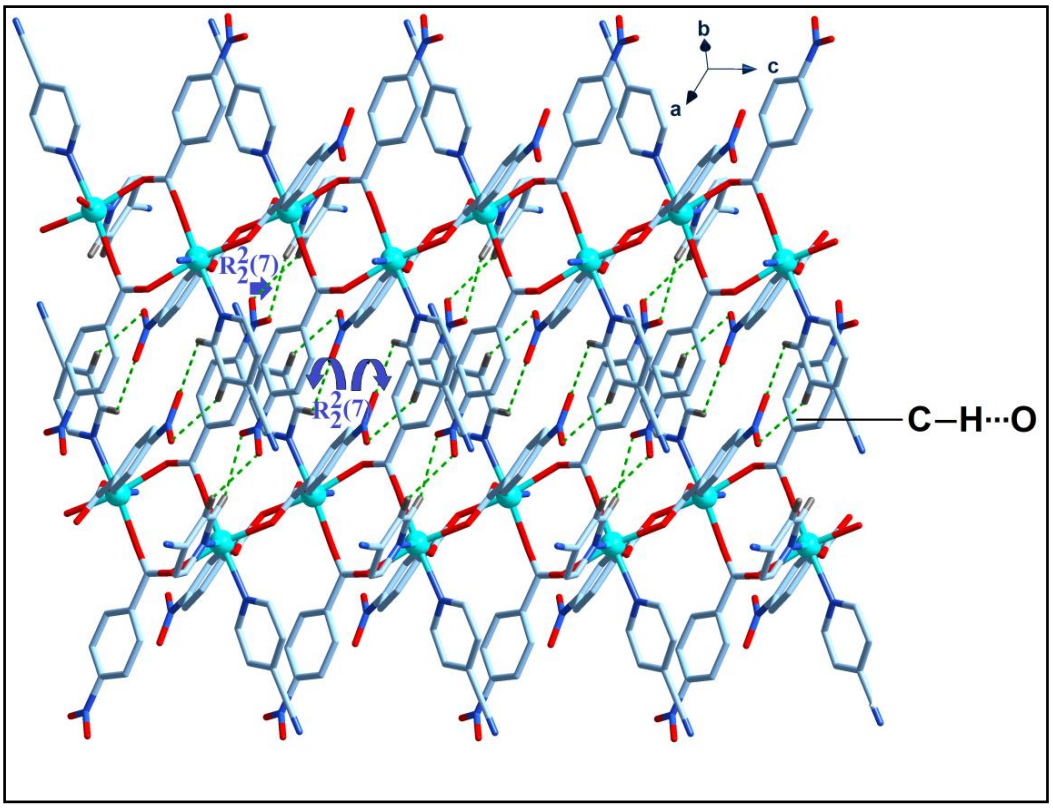

Figure 3.5(a) Connectivity of polymeric 1D chains of $[Mn(4\text{-NBz})_2(4\text{-CNpy})_2]_n$ (**4**) along *ac* plane via C–H···O interactions. Irrelevant hydrogen atoms and phenyl rings of *4-NBz* are omitted for clarity.

Along the *bc* plane, however, these chains, with the shortest inter-chain Mn···Mn distance of 12.15(22) Å are connected via the nitrile moieties of *4-CNpy* through a number of supramolecular interactions forming another supramolecular layer in the polymer. As seen from **Figure 3.5(b)**, the inter-chain space along this direction is

occupied by the nitrile groups from the coordinated *4-CNpy*. The –C≡N groups protruding out of one of the two *4-CNpy* moieties from two dimeric units in adjacent 1D chain are aligned in an anti-parallel manner. This perfect anti-parallel and inverse alignment of the nitrile groups may be an outcome of moderate π–π interactions, with the closest centroid to centroid distance of 3.393 Å between the π systems of two –C≡N fragments of the *4-CNpy*.[67] Interestingly, it may be pointed out that the C10–C13≡N2 angle is slightly smaller than the linearity (177.71°). This increased bending of the C10–C13≡N2 angle in **4** probably is an outcome of intermolecular interactions involving the nitrile groups attached to aromatic rings.

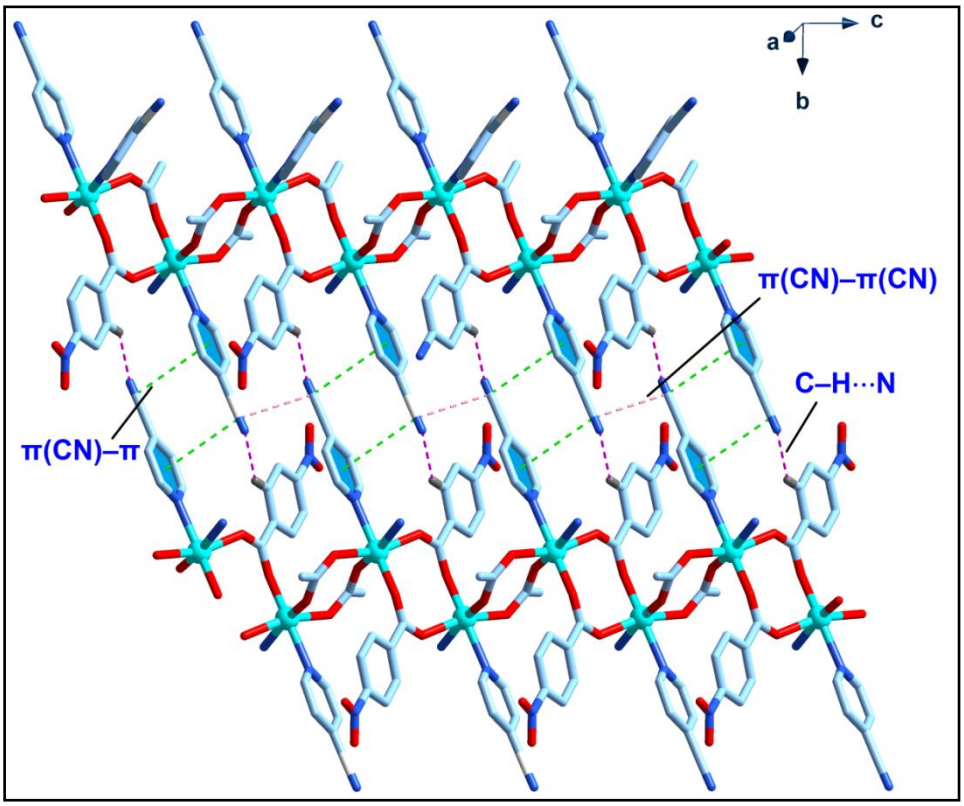

Figure 3.5(b) Connectivity of 1D chains of $[Mn(4\text{-}NBz)_2(4\text{-}CNpy)_2]_n$ (**4**) along *bc* plane via anti-parallel CN···CN, C–H···N and π(CN)···π interactions. Irrelevant hydrogen atoms and phenyl rings of *4-NBz* are omitted for clarity.

The anti-parallel alignment of the coordinated *4-CNpy* groups also results in another type of π–π interactions involving the π system of a nitrile group in a chain and the pyridine ring of the *4-CNpy* in adjacent chain at closest centroid-centroid distance of

3.665 Å. The polymeric 1D chain is also interconnected through weak C–H···NC hydrogen bonds that appear to play an important role in stabilizing the overall structure. The nitrile group of an individual *4-CNpy* present in a chain is hydrogen bond acceptor, forming interactions with the C7H7 moieties of *4-NBz* of adjacent chains. This hydrogen-bonding interaction has a C–H···N distance of 2.625 Å with corresponding C···N distances of 3.431 Å, consistent with the formation of weak hydrogen bonds.[68]

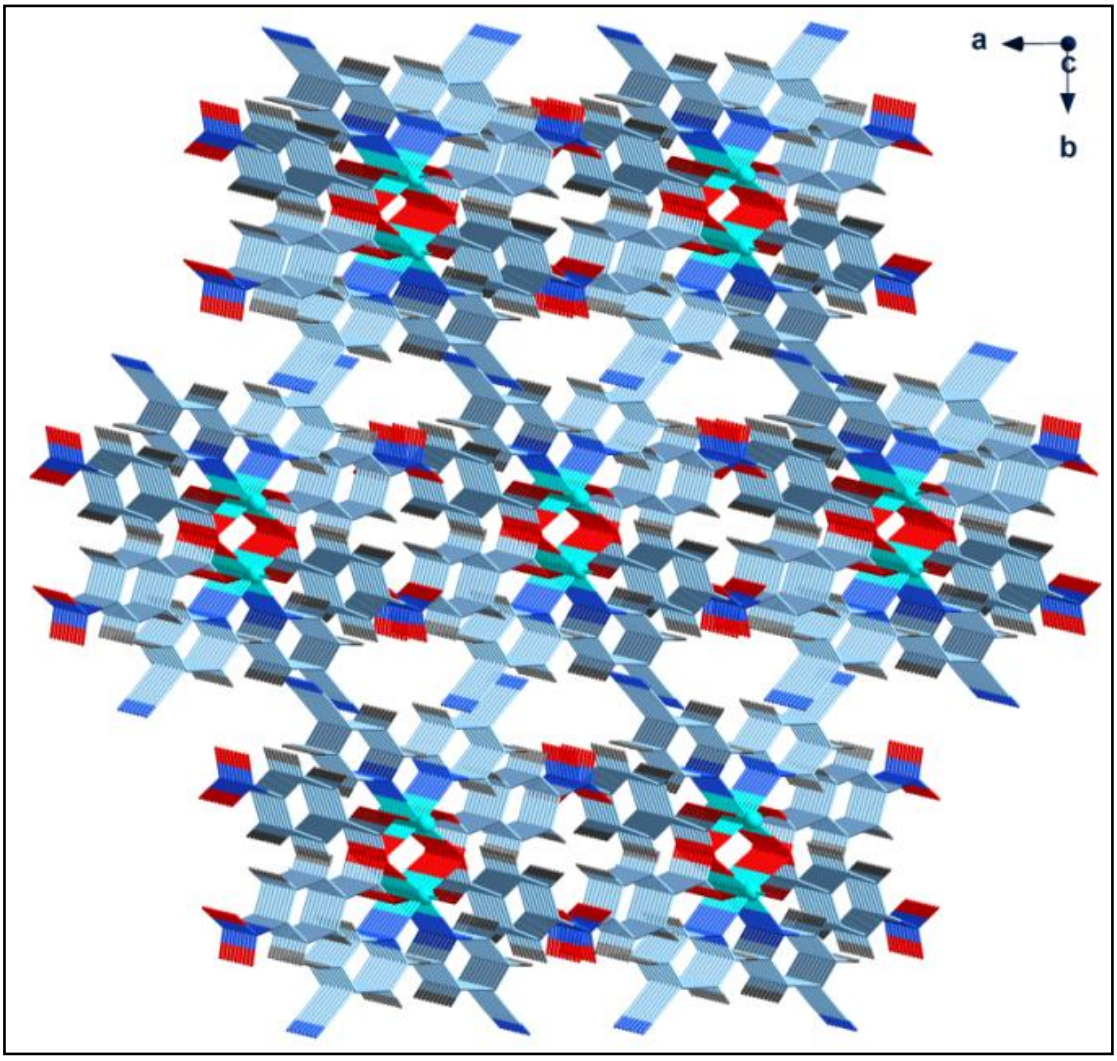

Figure 3.6 3D network structure of the polymer $[Mn(4\text{-}NBz)_2(4\text{-}CNpy)_2]_n$ (**4**) involving channels along crystallographic *c*-direction.

The supramolecular assembly of the polymeric 1D double chains along the *ac* and *bc* planes, aided by various supramolecular interactions involving the anti-parallel and

inverse nitrile fragments of coordinated *4-CNpy* results in a 3D network structure of **4** with interesting channels running along the *c*-direction, as shown in **Figure 3.6**.

3.3.3.2 Crystal structure of $[Mn(4\text{-}CNpy)_2(H_2BTC)_2]_n$ (5)

The basic unit of the polymeric complex **5** with the atom labeling scheme is shown in **Figure 3.7**. The selected bond lengths and bond angles of compound **5** are summarized in **Table 3.3**. The crystallographic analysis shows that complex **5** crystallizes in the triclinic $P\bar{1}$ space group. Unlike **4**, the crystal structure of the polymer **5** contains a basic trimeric unit $[Mn_3L_6L'_4]$ (where L = *4-CNpy* and L´ = H_2BTC^-) with Mn···Mn distances of 4.930 and 5.178 Å. A. Panja *et al*. have reported the Mn···Mn distances of 5.56 Å for a manganese coordination polymer *viz*. $[Mn(salen)Ag(CN)_2]_n$ [where, H_2salen = N,N´-bis(salicylidene)-1,2-diaminoethane)].[69] Compound **5** is in a *trans*-$[N_2O_4]$ surrounding core of four carboxylate oxygen atoms (O1, O2, O3, O4) from four bridging H_2BTC^- and two *4-CNpy* nitrogen atoms (N1, N3). The coordinated *4-CNpy* ligands containing N1 and N3 atoms are trans to each other. The root mean square (r.m.s.) deviations of their pyridine rings are 0.0472 and 0.1327 Å, respectively. The dihedral angle between the two pyridine rings is 66.8°. The four atoms in the equatorial plane of each Mn(II) centre have a r.m.s. deviation of 0.0446 Å. Similar to **4**, the bridging mode of the carboxylate group linking the Mn1 atom to its neighbouring Mn1A atom (A. 2–x, 2–y, 2–z) and Mn1B atom (B. 1−x, 2−y, 2−z) to make the tri-nuclear $[Mn_3(4\text{-}CNpy)_6(H_2BTC)_4]$ core is syn-syn with torsion angles of 6.82(98)° (O1−C10−O4A−Mn1A), 15.23(67)° (O1A−C10−O1−Mn1) and 101.95(39)° (O2−C1−O3B−Mn1B), 47.35(49)° (O3B−C1−O2−Mn1). S. J. Liu *et al*. have reported two similar isostructural complexes, $\{[M_2Cl_2(BTC)_{4/3}]\cdot(Me_2NH_2)^{+2}\cdot 4/3H_2O\}_n$ [M = Co(II), Mn(II)], where one of the carboxylate groups of BTC ligand bridges two metal atoms in the asymmetric unit in bidentate fashion, leaving the other two carboxylate groups free of coordination.[70] The twelve *cis*-angles [84.06(9)–100.41(9)°] and three *trans*-angles [174.42(9)–178.32(9)°] in compound **5** surrounding the central Mn1 atom deviate significantly from the ideal octahedral bond angles. Also, the average equatorial bond lengths (2.1446 Å) are smaller than the average axial bond lengths (2.294 Å) in complex **5** indicating a *z*-out type tetragonal distortion from the ideal octahedral geometry of the central atom similar to **4**.[71]

Table 3.3 Selected bond lengths and angles (Å and °) for compound **5**.

Bond	d, Å	Angle	Degree (°)
Mn1–O1	2.1183(2)	N1–Mn1–O3	87.99(8)
Mn1–O2	2.1520(3)	N1–Mn1–O2	90.03(9)
Mn1–O3	2.1598(2)	N1–Mn1–N3	178.32(9)
Mn1–O4	2.1483(3)	N1–Mn1–O1	89.98(9)
Mn1–N1	2.2871(2)	N1–Mn1–O4	93.28(9)
Mn1–N3	2.3009(2)	O3–Mn1–O2	91.10(8)
		O3–Mn1–N3	92.30(8)
		O3–Mn1–O1	174.75(9)
		O3–Mn1–O4	84.54(9)
		O2–Mn1–N3	88.31(9)
		O2–Mn1–O1	84.06(9)
		O2–Mn1–O4	174.42(9)
		N3–Mn1–O1	89.59(9)
		N3–Mn1–O4	88.39(9)
		O1–Mn1–O4	100.41(9)

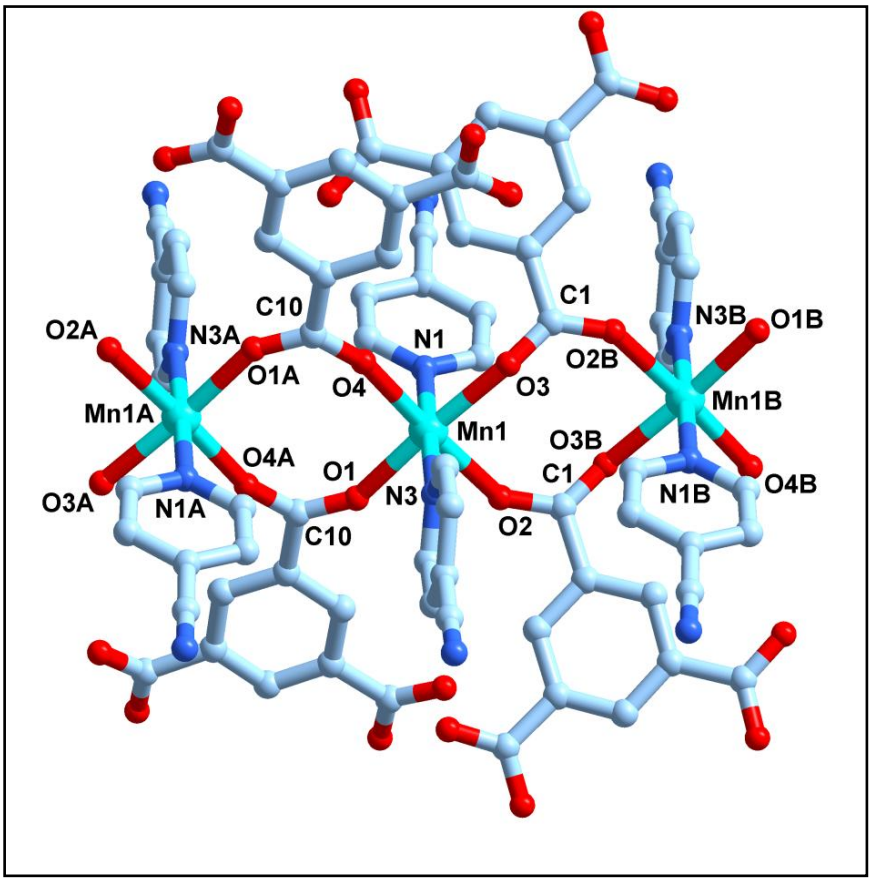

Figure 3.7 View of the coordination environment of Mn(II) centers in $[Mn(4\text{-}CNpy)_2(H_2BTC)_2]_n$ (**5**). All hydrogen atoms are omitted for clarity. Symmetry codes: A. 2–x, 2–y, 2–z; B. 1–x, 2–y, 2–z.

In the crystal structure of polymer **5**, the $[Mn(4\text{-}CNpy)_2(H_2BTC)_2]$ units are interconnected through the bridging H_2BTC^-, thereby forming a polymeric 1D double-chain that extends along the crystallographic *a*-direction (**Figure 3.8**).

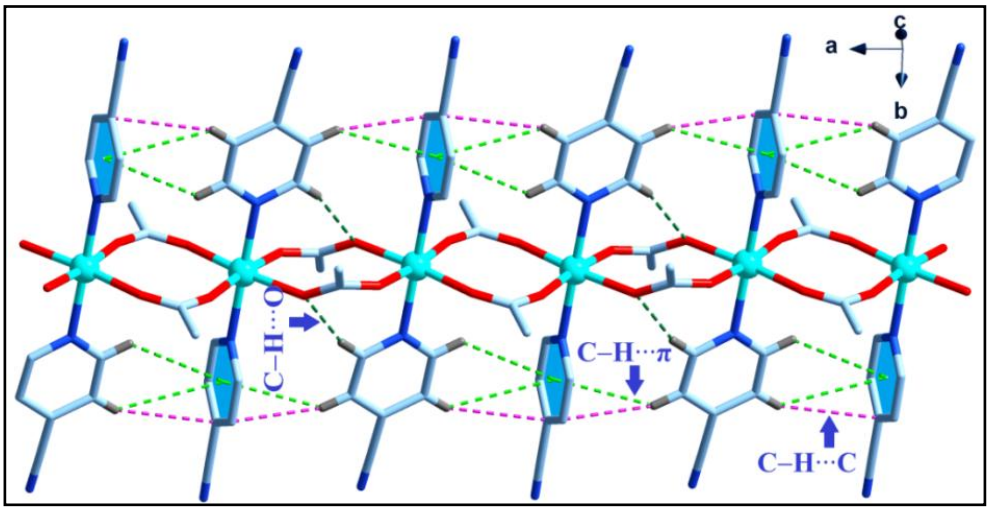

Figure 3.8 Polymeric1D double-chain of $[Mn(4\text{-}CNpy)_2(H_2BTC)_2]_n$ (**5**) featuring adjacent $[Mn(4\text{-}CNpy)_2(BTC)_2]$ units along *a*-direction. Irrelevant hydrogen atoms and BTC ligands are omitted for clarity.

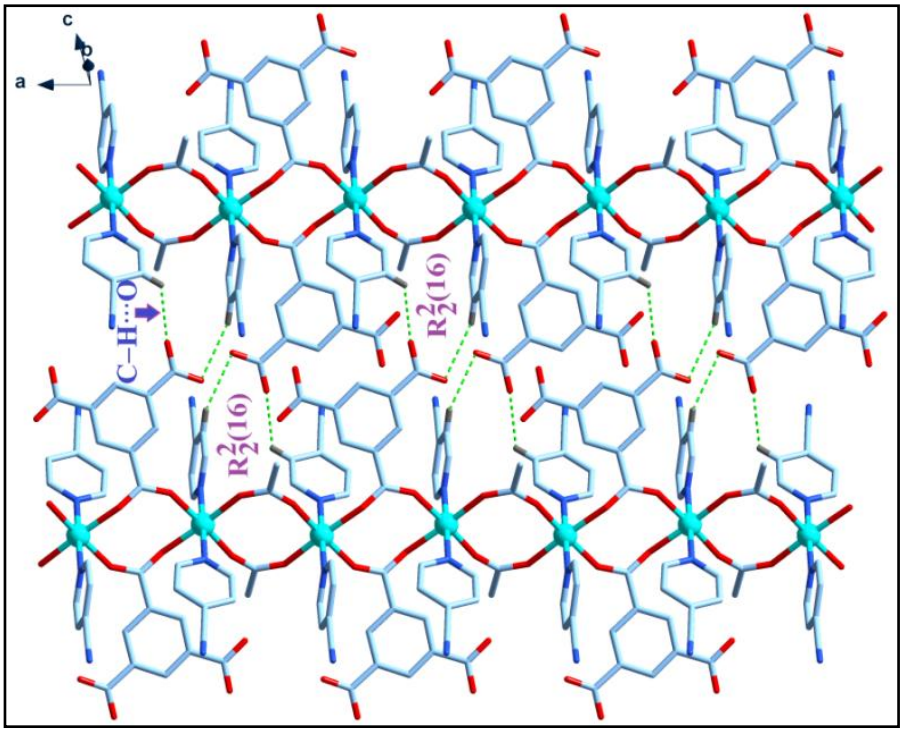

(**a**)

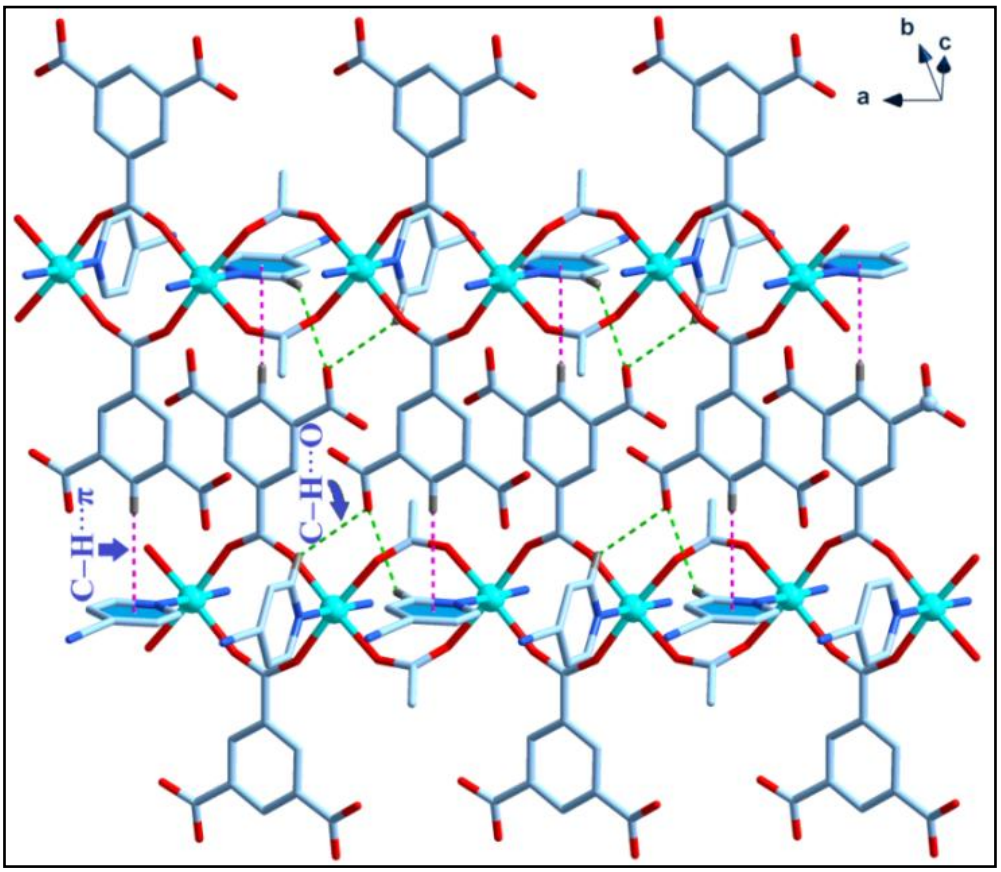

(**b**)

Figure 3.9 Connectivity of 1D double-chain in $[Mn(4\text{-}CNpy)_2(H_2BTC)_2]_n$ (**5**) via *H_2BTC* along the *ac* plane via (a) C–H···O and (b) C–H···π interactions involving *H_2BTC* moieties. Irrelevant hydrogen atoms and BTC ligands are omitted for clarity.

The 1D chain of **5** is stabilized by a number of supramolecular interactions. The C30H30 and C42H42 moieties of the *4-CNpy* containing N1 and N2 atoms point towards the pyridyl π-cloud centroid of the adjacent *4-CNpy* containing N3 and N4 atoms, forming C–H···π interactions (**Figure 3.8**) with C–Cg distances of 3.278 Å and 3.323 Å respectively.[72] The C029–H029 moiety of the *4-CNpy* on opposite direction of the latter forms another C–H···π interaction with C–Cg distance of 3.064 Å. C. Zhu *et al*. have also reported C–H···π interactions with C–Cg distances 3.554 Å in a Cr(III) complex based on 2-substituted 8-hydroxyquinoline ligands, namely $[Cr(L_1)_3]$, (HL_1 = (E)-2-[2-(4-nitro-phenyl)-vinyl]-8-hydroxy-quinoline).[73] The 1D chain of **5** is additionally stabilized by an inter chain C–H···O interaction between the pyridyl –CH

moiety of the *4-CNpy* and the coordinated O3 atom of a bridging BTC carboxylate moiety, with a C–O distance of 3.511 Å (**Table 3.5**). Most striking feature in the 1D chain of **5**, however, is the pair wise parallel alignment of *4-CNpy* of Mn(II) units of the polymeric chain, resulting in acidic pyridyl C–H donor groups of *4-CNpy* apparently interacting with the carbon acceptor atoms of two neighbouring ones (**Figure 3.8**), thereby forming two weak intermolecular C–H···C contacts (**Table 3.4**).

Table 3.4 Geometry of C–H···C contacts in **5**.

C–H···C	D(Å)	d(Å)	θ(°)
C29–H29···C20	3.808	2.925	159.19
C42–H42···C041	3.991	3.150	151.26

The polymeric double-chains in **5** are interconnected via weak C–H···O and C–H···π interactions involving H_2BTC^-, resulting in the formation of a 2D layer running in the *ac* plane [**Figure 3.9(a)**]. The C–H···O interaction involves the C19H19 moiety of *4-CNpy* and the uncoordinated carboxyl oxygen atom (O8) with donor-acceptor distance of 3.464 Å [**Figure 3.9(a)**]. M. B. Nasr and his group have reported weak C–H···O interactions with donor-acceptor distance ranging from 3.2 to 3.4 Å for a new coordination complex *viz*. $[CuClO_4(C_4H_6N_2O)4H_2O]ClO_4(C_4H_6N_2O)_{0.08}$ (where $C_4H_6N_2O$ = dihydropyrimidinone).[74] However, 1D chains of **5** are joined together by two inter chain C–H···O associations between the C40H40 and C42H42 moieties from two different neighboring *4-CNpy* molecules in one chain with the uncoordinated carboxyl oxygen atoms (O5 and O6) from the same H_2BTC^- in another chain, having C–H···O distances of 2.764 Å and 2.416 Å respectively. These two C–H···O associations give rise to $R_2^2(16)$ type supramolecular rings [**Figure 3.9(a)**]. The C14H14 moiety of H_2BTC^- in one chain points to the centroid of the pyridyl ring of *4-CNpy* in another chain, thereby forming C–H···π interactions with C–Cg distance of 3.148 Å [**Figure 3.9(a)**].

The 1D double-chains of **5**, with the shortest inter chain Mn···Mn distance of 14.39(41) Å, are connected via the nitrile moieties of the coordinated *4-CNpy* through a number of supramolecular interactions along the *ab* plane forming another supramolecular layer in the polymer. As **Figure 3.10** reveals, the inter chain space along this direction is occupied by the nitrile groups from the coordinated *4-CNpy* of the

complex. The –C≡N groups protruding out of the two *4-CNpy* moieties around each Mn(II) centre in adjacent 1D chains are aligned in an anti-parallel manner. This alignment of the nitrile groups gives rise to moderate π–π interactions, with the closest centroid to centroid distances of 3.446 Å, 3.460 Å and 3.945 Å between the π systems of two adjacent –C≡N fragments of the *4-CNpy*. Similar to compound **4**, due to these intermolecular interactions between the nitrile functional groups attached to aromatic rings, the C31–C45≡N2 and C41–C46≡N4 angles deviate from linearity (178.77° and 178.42° respectively). Along this direction, the polymeric 1D chains are further interconnected through weak C–H···N hydrogen bonds (2.823 Å, 120.50°) from the pyridyl *H* atom in one chain to the N2 acceptor in another. With all these supramolecular interactions involving the H_2BTC^- as well as the *4-CNpy* in the two planes with almost perpendicular directions, the polymeric chains in **5** build up an interesting 3D architecture (**Figure 3.11**).

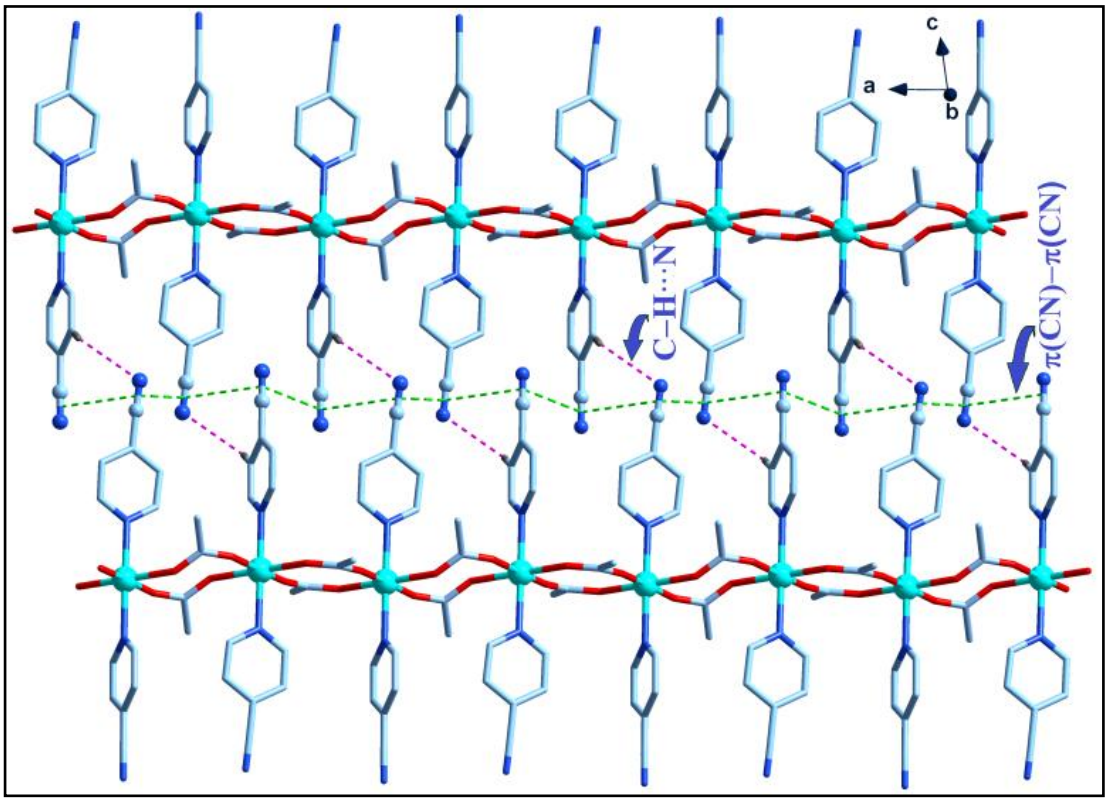

Figure 3.10 Connectivity of 1D double chain in $[Mn(4\text{-}CNpy)_2(H_2BTC)_2]_n$ (**5**) via CN···CN contacts between *4-CNpy* along the *ab* plane. Irrelevant hydrogen atoms and H_2BTC^- are omitted for clarity.

Table 3.5 Selected hydrogen bond distances (Å) and bond angles (°) for compounds **4**, **5** and **6**.

	D–H···A	d(D–H)	d(D–A)	d(H···A)	<(DHA)
4	C7–H7···N2[a]	0.930	3.431	2.625(2)	147.37(1)
	C8–H8···O2[b]	0.930	3.434	2.798(2)	126.53(2)
5	C9–H9···O1[b]	0.930	3.474	2.608(8)	155.26(3)
	C20–H20···N2[c]	0.930	3.391	2.823(4)	120.50(2)
	C19–H19···O8	0.929	3.437	2.858(3)	123.97(2)
	C025–H025···O8[d]	0.929	3.167	2.820(4)	103.41(2)
6	O4–H4B···O11	1.015	2.821(1)	1.854(1)	158.12(3)
	O2–H2B···O13	0.847(3)	2.915(5)	2.074(3)	171.43(3)
	O9–H9B···O4[d]	0.780	2.796(1)	2.039(1)	163.63(5)
	O6–H6A···O3[e]	0.890(3)	2.736(5)	1.849(40)	174.49(2)
	O18–H18A···Ol[f]	0.887(3)	2.786(5)	1.904(30)	172.33(2)
	O4–H4A···O5[f]	0.940	2.757(1)	1.820(1)	174.44(4)
	O16–H16A···O2[g]	0.838(3)	2.751(5)	1.926(39)	167.57(3)
	O1–H1A···O20[h]	0.934(3)	2.828(4)	1.943(3)	157.30(2)
	O3–H3A···O5[i]	0.913(4)	2.892(5)	2.003(30)	164.24(2)
	C40–H40···N1[g]	0.930(7)	3.522(9)	2.755(68)	140.39(4)

Symmetry codes: a. –x–1/2, –y+1/2+1, –z+1; b. –x–1,+y, –z+1/2+1; c. x,+y+1, +z–1; d. x,+y–1,+z; e. x–1/2, –y+1,+z; f. x+1/2, –y+1,+z; g. x,+y+1,+z; h. x–1/2, –y+2,+z; i. x+1/2, –y,+z.

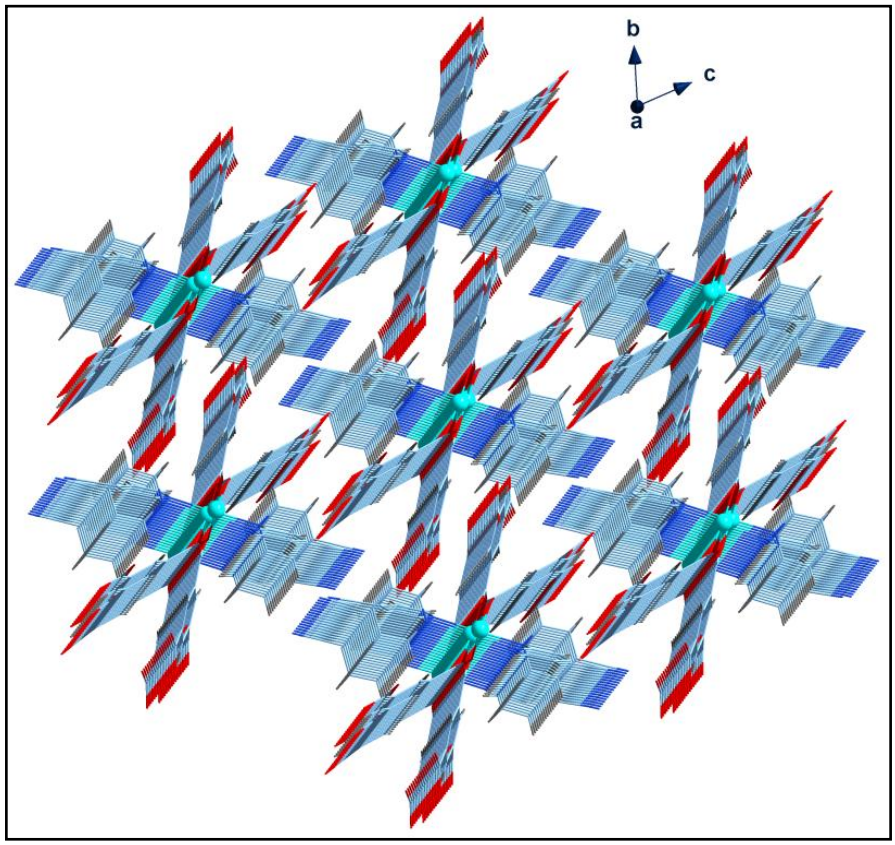

Figure 3.11 View of the 3D framework of $[Mn(4\text{-}CNpy)_2(H_2BTC)_2]_n$ (**5**).

3.3.3.3 Theoretical studies of complexes $[Mn(4\text{-}NBz)_2(4\text{-}CNpy)_2]_n$ (4) and $[Mn(4\text{-}CNpy)_2(H_2BTC)_2]_n$ (5)

As commented above, we have focused the theoretical study to analyze the interesting 2D assemblies that are generated by means of anti-parallel CN···CN interactions, as shown in **Figure 3.5(b)** for compound **4** and **Figure 3.10** for compound **5**. We are particularly interested to study the strength of the interaction and the influence of the coordination of the *4-CNpy* to Mn(II) upon the binding energy. To rationalize the interaction from an electrostatic point of view, we have first computed the molecular electrostatic energy (MEP) surface of *4-CNpy* [**Figure 3.12(a)**] and also its complex to the Mn(II) metal centre [**Figure 3.12(b)**], which is charge-balanced by two additional formate ligands to keep the model neutral.

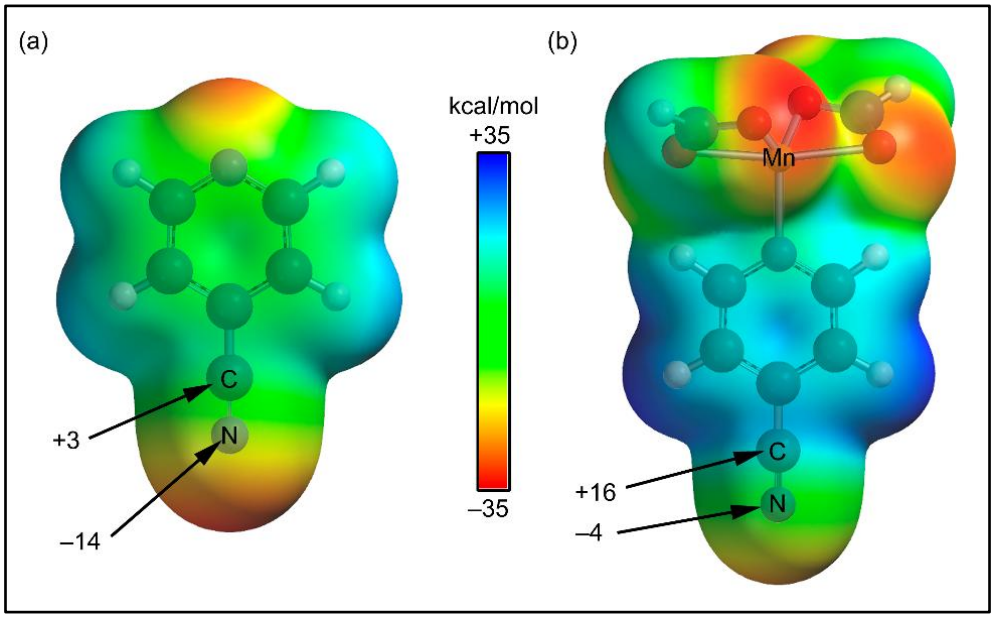

Figure 3.12 Molecular electrostatic potential (MEP) surface of *4-CNpy* (**a**) and its complex with Mn(II) (**b**) (isosurface value 0.001 a.u.). The MEP energies at the selected points are also indicated in kcal/mol.

The plot of MEP onto the van der Waals surface in *4-CNpy* reveals a slightly positive MEP value over the C atom of the C≡N group (+3 kcal/mol) and a significantly negative value over the N atom (–14 kcal/mol), thus explaining the tendency to form anti-parallel stacking interactions. The plot of the MEP surface in the Mn(II) model complex involving 4-CNpy [**Figure 3.12(b)**] shows that the MEP value over the C atom increases significantly (+16 kcal/mol) and the MEP value over the N atom is reduced

(in absolute value) considerably. Therefore, the nature of the CN···CN interaction changes drastically upon coordination from an electrostatic point of view. That is, the CN group is more electrophilic than nucleophilic/basic upon coordination.

In **Figure 3.13(a)**, we show a partial view of the X-ray solid state of compound **4** where the anti-parallel CN···CN interactions are indicated. Due to the polymeric nature of this compound, we have used a theoretical model (monomeric unit) where the Mn is coordinated to two *4-CNpy*, two *4-NBz* and two formic acids as ligands in order to mimic the coordination sphere of the metal as it has in the solid state and also to keep the size of the system computationally affordable [**Figure 3.13(b)**]. The interaction energy of the dimer governed by CN···CN contacts is ΔE_1 = –4.3 kcal/mol, thus confirming the attractive nature of the interaction. We have also evaluated the interaction energy of the dimer without the coordination of the ligand to the Mn(II) ions [**Figure 3.13(c)**] and the binding energy is reduced to ΔE_1 = –3.9 kcal/mol, thus revealing that the CN···CN interaction strengthens upon coordination.

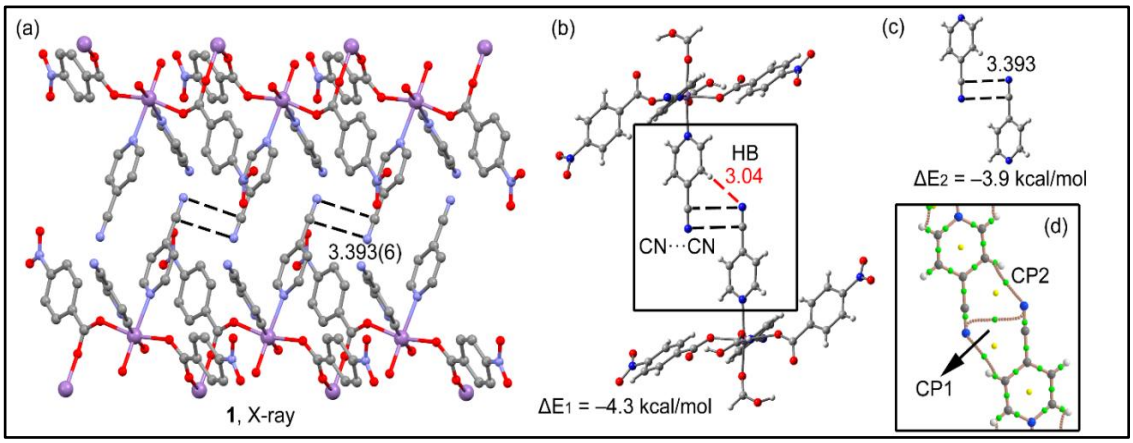

Figure 3.13(a) Partial view of the X-ray structure of $[Mn(4\text{-}NBz)_2(4\text{-}CNpy)_2]_n$ (**4**); (**b**,**c**) Theoretical models; (**d**) AIM distribution of bond and ring critical points (green and yellow spheres respectively) and bond paths of the theoretical model. Distances are in Å.

We have also computed the distribution of critical points and bond paths in the dimer. The existence of a bond critical point and bond path connecting two atoms is a clear indication of interaction.[75] The AIM analysis is represented in **Figure 3.13(d)** and it can be observed that the anti-parallel CN···CN interaction is characterized by the presence of a bond CP (green sphere) and bond path connecting both N atoms of the CN

groups. Unexpectedly, it also shows two bond critical points and bond paths symmetrically distributed connecting two aromatic C–H bonds to the N atoms of the CN groups [denoted as CP2 in **Figure 3.13(d)**]. Therefore, this long H-bond [HB, represented in red in **Figure 3.13(b)**] also contributes to the stabilization of the assembly. The density at the critical point can be considered as a measure of the strength of the interaction. The ρ(r) value at CP1 is 0.005 a.u. and at CP2 is 0.004 a.u., therefore the CN···CN interaction is likely stronger than the H-bond, as expected by the long H···N distance (3.04 Å).

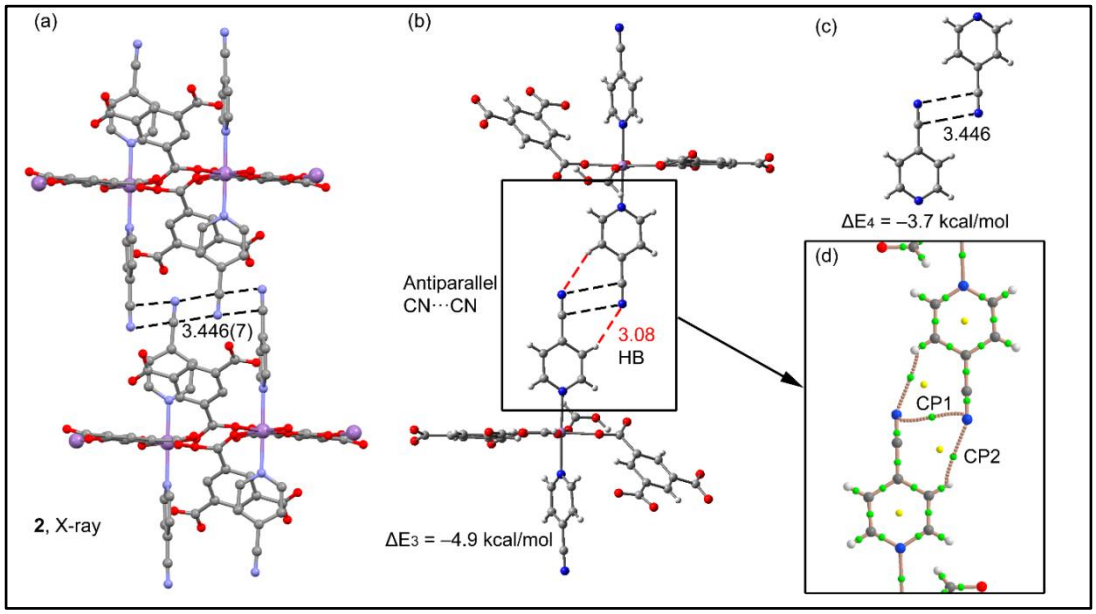

Figure 3.14(a) Partial view of the X-ray structure of $[Mn(4\text{-}CNpy)_2(H_2BTC)_2]_n$ (**5**); (**b**,**c**) Theoretical models; (**d**) AIM distribution of bond and ring critical points (green and yellow spheres respectively) and bond paths of the theoretical model. Distances are in Å.

For compound **5**, we have performed a similar DFT/AIM study. In **Figure 3.14(a)**, we show a partial view of its X-ray solid state structure where the anti-parallel CN···CN interactions are indicated as dashed lines. Since this compound is also polymeric, we have used a theoretical model (monomeric unit) where the Mn(II) is coordinated to two *4-CNpy*, two BTC units and two formic acids in order to keep the octahedral coordination sphere of the metal [**Figure 3.14(b)**]. The interaction energy of the dimer governed by the CN···CN interactions is ΔE_3 = –4.9 kcal/mol, which is

comparable to that obtained for compound **4**. In this dimer, two symmetrically equivalent H-bonds are also established [long distance of 3.08 Å, red dashed lines in **Figure 3.14(b)**]. We have also evaluated the interaction energy of the dimer without the coordination of the ligand to the Mn(II) ions [**Figure 3.14(c)**] and the binding energy is reduced to ΔE_4 = –3.7 kcal/mol, thus confirming that the CN···CN interaction strengthens upon coordination. The AIM analysis of compound **5** is represented in **Figure 3.14(d)** and it can be observed that the anti-parallel CN···CN interaction is characterized by the presence of a bond CP (green sphere) and bond path connecting both N atoms of the CN groups. It also shows two bond critical points and bond paths symmetrically distributed connecting two aromatic C–H bonds to the N atoms of the CN groups (denoted as CP2) confirming the existence of the long H-bonds. The ρ(r) value at CP1 is 0.005 a.u. (identical to that obtained for compound **4**) and at CP2 is reduced to 0.003 a.u. compared to compound **4**, in agreement with the longer H···N distance (3.08 Å) observed in compound **5**.

3.3.3.4 Crystal structure of [$Mn(Bz)_2(H_2O)_4$](4-CNpy)·$2H_2O$ (**6**)

Single-crystal X-ray analysis reveals that complex **6** crystallizes in the orthorhombic crystal system with space group *P*ca2_1. The details of single crystal XRD and structure refinement data for **6** are given in **Table 3.1**. There are two crystallographically unique Mn(II) ions, four coordinated *Bz* anions, eight aqua molecules in the asymmetric unit of **6**. Along with this, the asymmetric unit has two *4-CNpy* and four water molecules in the lattice. As shown in **Figure 3.15**, each Mn(II) ion is octahedrally coordinated by six oxygen atoms (O6, O7, O8, O9, O10 and O12 for Mn1 and O14, O15, O16, O17, O18 and O19 for Mn2). Out of these, two O atoms are from two *Bz* moieties while the other four are from four aqua ligands. The twelve *cis*-angles [80.89(13)–102.17(11)° and 80.15(13)–101.55(12)° in the Mn1 and Mn2 units, respectively] and three *trans*-angles [168.67(13)–172.47(14)° and 169.03(13)–173.38(14)° in Mn1 and Mn2 units respectively] show significant deviations from the ideal octahedral bond angles. Similarly, the average Mn–O axial bond lengths [2.1711 Å and 2.1735 Å in the Mn1 and Mn2 units, respectively] are somewhat shorter than the average Mn–O equatorial bond lengths [2.1853 and 2.1775 Å in the Mn1 and Mn2 units, respectively]. These deviations indicate a *z*-in type tetragonal distortion from the

ideal octahedral geometry of the central atoms in both units.[76] Furthermore, the Mn–O_{Bz} bond lengths are comparable to the corresponding bond lengths in the literature.[77,78] The *Bz* moieties around the metal centers are nearly planar in both the complex units. The least squares plane of the atoms Mn1, O7, O8, O10 and O12 has a r.m.s. deviation of 0.0154 Å. This value is 0.0133 Å for the atoms Mn2, O14, O15, O17 and O19. The Mn(1)···Mn(2) distance in the open supramolecular dimer is found to be 15.731 Å, which is much larger than the Mn···Mn distance found in dimeric compounds reported earlier.[77] G. Cui and his group have reported two crystallographically independent Cu(II) ions in $[Cu_2(btec)(btx)_{1.5}]$ [where, btec = 1,2,4,5-benzenetetracarboxylate and btx = 1,4-bis(1,2,4-triazol-1-ylmethyl)benzene] with a Cu(1)···Cu(2) distance of 3.228(8) Å.[79] A. Gogoi *et al*. have also recently reported a supramolecular open dimer, $[Co(bpy)(Hpht)(H_2O)_3][Co(bpy)(pht)(H_2O)_2]Cl.2H_2O$ (bpy = 2,2'-bipyridine; Hpht, pht = o-phthalate anions) with Co(1)···Co(2) distance of 5.02(8) Å.[80] The selected bond lengths and bond angles for **6** are presented in **Table 3.6**.

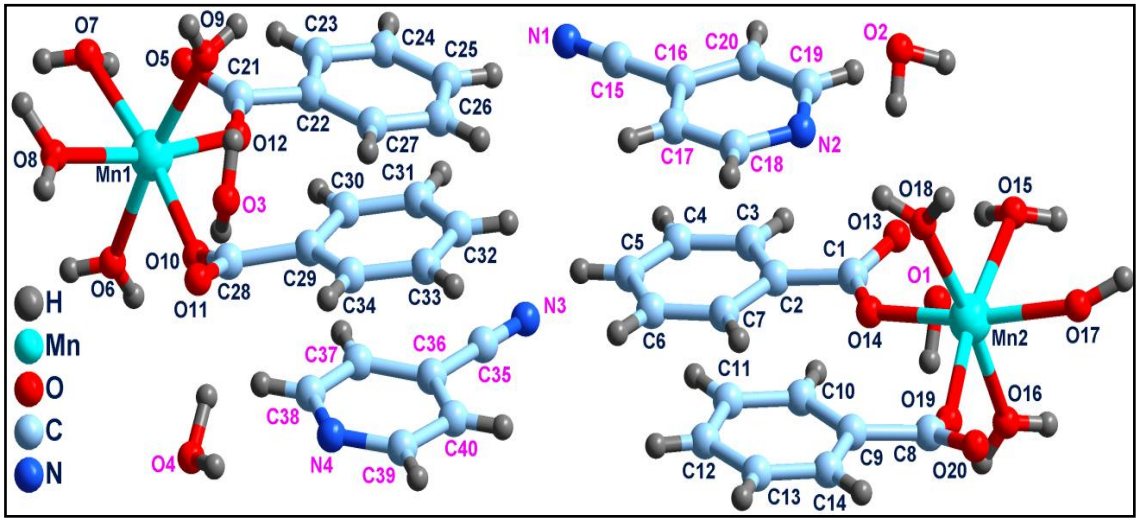

Figure 3.15 Molecular structure of $[Mn(Bz)_2(H_2O)_4](4\text{-}CNpy)\cdot 2H_2O$ (**6**).

In the crystal packing of **6**, the two crystallographically unique Mn(II) complex units are interconnected via four π–π, three C–H···N and two O–H···N interactions (**Figure 3.16**). Two lattice *4-CNpy* molecules from neighbouring complexes play an important role in stabilizing the complex units involving Mn(II) centers to form a

supramolecular open dimer.[81] Aromatic π–π interactions are observed between different pyridyl rings of lattice *4-CNpy* and phenyl groups of coordinated benzoates at a centroid–centroid separation of 3.743 Å, 3.760 Å, 3.827 Å and 3.779 Å for the open dimer involving Mn(II) complex units. Such π–π interactions [centroid–centroid separation of 3.6925(1) Å] involving pyridyl rings are reported by Di Sun *et al*. in [Ag(*CNpy*)$_2$(Hpta)] [where, *CNpy* = 4-cyanopyridine, H_2pta = phthalic acid].[82] The distances of intramolecular π-π interactions in the compound are 3.480(3), 3.560(3), 3.612(3), 3.639(2) Å. The open dimer in compound **6** is held via two types of C–H···N interactions: (i) One involving the two *4-CNpy* molecules in the lattice with C40–H40···N1 distance of 2.756 Å; (ii) The second C–H···N interaction involves the phenyl ring of the carboxylate group and the nitrile moiety of the *4-CNpy* molecule in the lattice with C26–H26···N1 distance of 2.889 Å. Interestingly, two types of O–H···N interactions are also observed between lattice *4-CNpy* and coordinated aqua ligands of Mn(II) centers with O18–H18B···N2 and O9–H9A···N4 distances of 2.006 Å and 2.020 Å respectively.

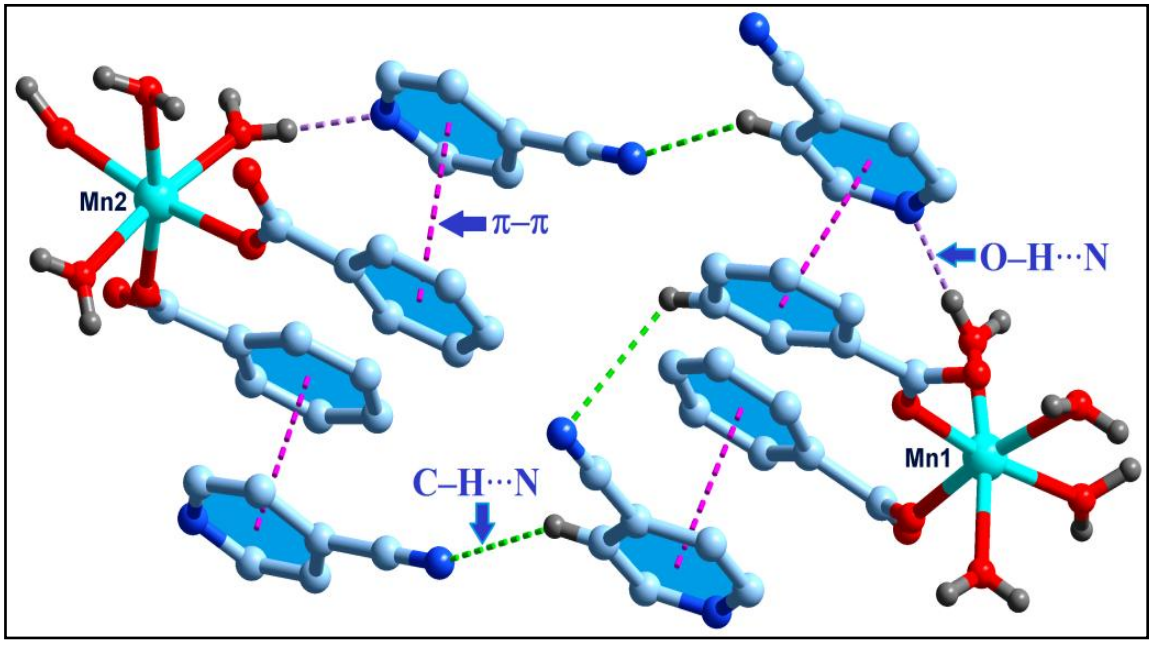

Figure 3.16 A view of the supramolecular open dimer involving two independent Mn(II) centers formed through O–H···N, C–H···N and π–π interactions in [Mn(Bz)$_2$(H_2O)$_4$](4-CNpy)·2H_2O (**6**). Irrelevant aromatic H-atoms are omitted for clarity.

Table 3.6 Selected bond lengths and bond angles (Å and °) for complex **6**.

Bond	d, Å	Angle	Degree (°)
Mn1–O6	2.1744(3)	O9–Mn1–O6	172.47(1)
Mn1–O7	2.2472(3)	O9–Mn1–O7	92.47(1)
Mn1–O8	2.1772(3)	O9–Mn1–O8	94.13(1)
Mn1–O9	2.1678(3)	O9–Mn1–O10	89.83(1)
Mn1–O10	2.1641(3)	O9–Mn1–O12	86.10(1)
Mn1–O12	2.1528(3)	O8–Mn1–O6	91.92(1)
		O8–Mn1–O7	80.89(1)
		O8–Mn1–O10	89.17(1)
		O8–Mn1–O12	168.67(1)
		O6–Mn1–O7	92.91(1)
		O6–Mn1–O10	85.77(1)
		O6–Mn1–O12	88.85(1)
		O10–Mn1–O7	169.93(1)
		O10–Mn1–O12	102.17(1)
		O7–Mn1–O12	87.77(1)
Mn2–O14	2.1501(3)	O18–Mn2–O16	173.38(1)
Mn2–O15	2.2474(3)	O18–Mn2–O14	85.53(1)
Mn2–O16	2.1747(3)	O18–Mn2–O15	91.73(1)
Mn2–O17	2.1677(3)	O18–Mn2–O17	94.17(1)
Mn2–O18	2.1723(4)	O18–Mn2–O19	90.13(1)
Mn2–O19	2.1449(3)	O19–Mn2–O16	86.09(1)
		O19–Mn2–O14	101.55(1)
		O19–Mn2–O15	169.49(1)
		O19–Mn2–O17	89.40(1)
		O16–Mn2–O14	89.92(1)
		O16–Mn2–O15	92.97(1)
		O16–Mn2–O17	91.22(1)
		O17–Mn2–O14	169.05(1)
		O17–Mn2–O15	80.15(1)
		O14–Mn2–O15	88.92(1)

The most interesting feature of the crystal packing in **6** is the formation of a host Mn(II) supramolecular tetramer (**Figure 3.17**). Such supramolecular tetrameric assembly was reported by S. S. Sreejith and his group in a novel Zn(II) inclusion complex (with guest water molecule) of 6,6′-diethoxy-2,2′-[2,2-dimethylpropane-1,3-diylbis(nitrilomethylidyne)]-diphenol salen-type Schiff base.[83] The enclathrated water molecules (O1 and O3) in the Mn(II) host units in compound **6** result in the tetramer through the coordinated *Bz* moieties of the two complex units via weak C–H···C contacts [C(sp^2)–H···C(sp^2), (C–C = 3.952 Å].[84]

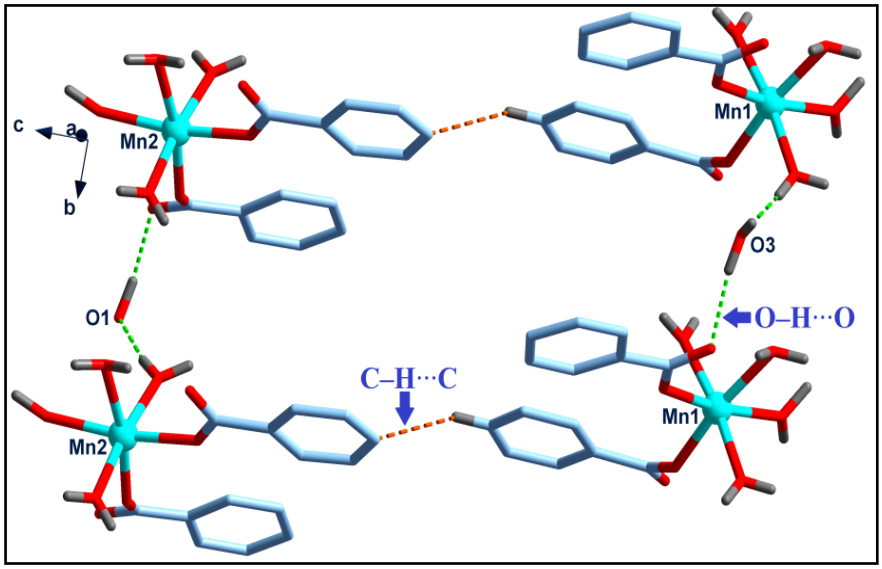

Figure 3.17 Supramolecular tetramer of Mn(II) host units in compound **6** with enclathrated water molecules involving C–H···C contacts. Irrelevant aromatic H-atoms are omitted for clarity.

The two guest *4-CNpy* molecules in the supramolecular host tetramer are enclathrated via π–π interaction between the phenyl moiety of the benzoate and the pyridyl ring of the *4-CNpy* molecules, resulting in a 2D architecture along the *bc* plane [**Figure 3.18(a)**]. The nitrile nitrogen atom of guest *4-CNpy* molecule is involved in weak C–H···N interaction with coordinated *Bz* of Mn(2) centre with donor acceptor distance of 3.469 Å, which also contributes to the stability of the supramolecular tetramer [**Figure 3.18**]. S. Nasri *et al*. have also reported such C–H···N interactions involving *4-CNpy* having donor acceptor distance of 3.2 to 3.4 Å in [Zn(TPBP)(*4-CNpy*)]*4-CNpy* [where TPBP = 5,10,15,20-(tetraphenylbenzoate)porphyrinate].[85] The range of the D–H–A angles and H–A and D–A distances (D: Donor; A: Acceptor) are represented in **Table 3.5**.

Lattice water molecules involving O2 and O4 atoms play an important role in stabilizing the Mn(II) units of compound **6**. The lattice water molecule (O2) connects two Mn2 units via two different O–H···O hydrogen bonds involving the coordinated water molecule from one unit and the non-coordinated carboxylate O-atom of the other (O2–H2B···O13 and O16–H16A···O2 distances of 2.0738 and 1.925 Å respectively) along the *bc* plane [**Figure 3.19(a)**]. The other lattice water molecule (O4) connects three neighbouring Mn1 units via O–H···O hydrogen bonds along the *ab* plane, which

also contributes towards the stability of supramolecular architecture of compound **6** [**Figure 3.19**(**b**)].

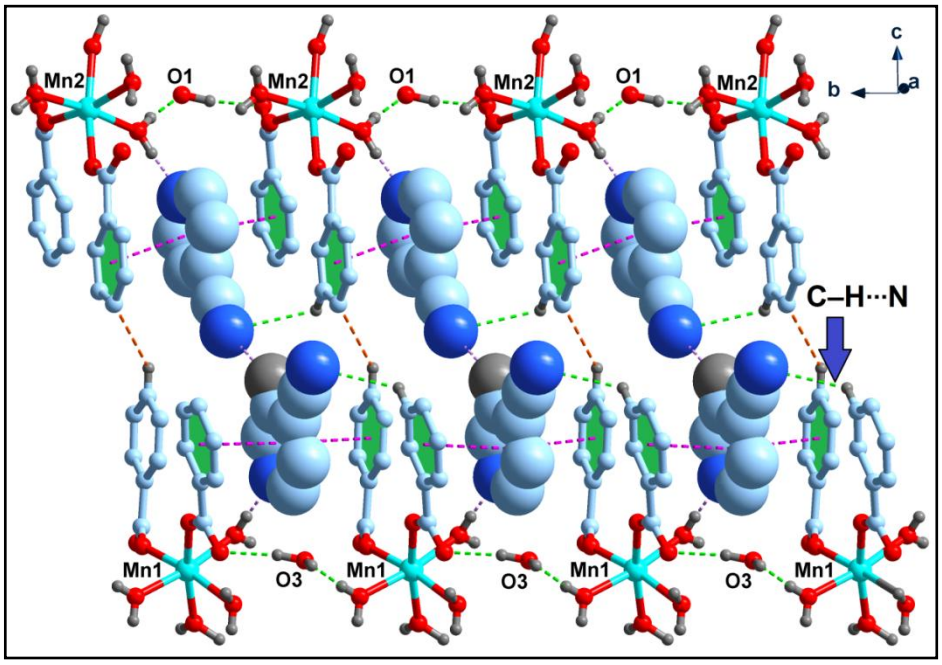

(**a**)

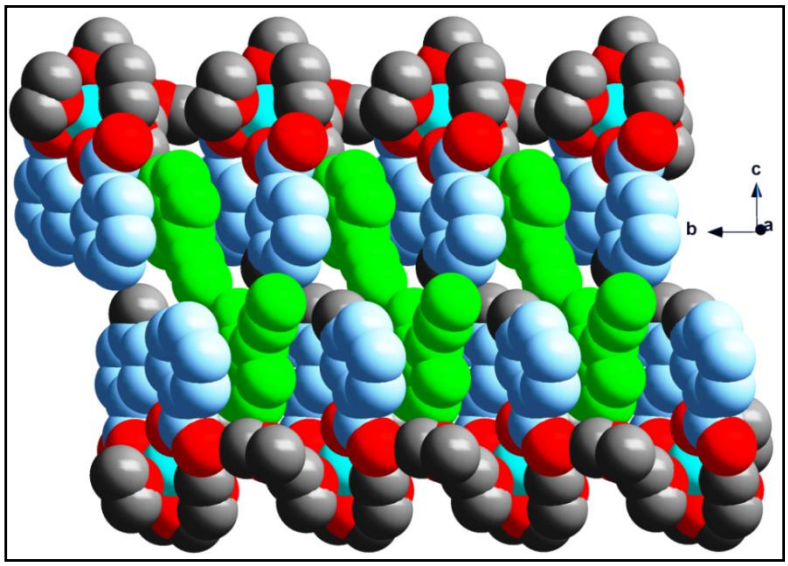

(**b**)

Figure 3.18(**a**) 2D array of **6** involving C–H···C contacts along the *bc* plane; (**b**) Space-filling representation showing enclatharation of *4-CNpy* molecules in the supramolecular host tetramer of compound $[Mn(Bz)_2(H_2O)_4](4\text{-}CNpy)\cdot 2H_2O$ (**6**). Irrelevant aromatic H-atoms are omitted for clarity.

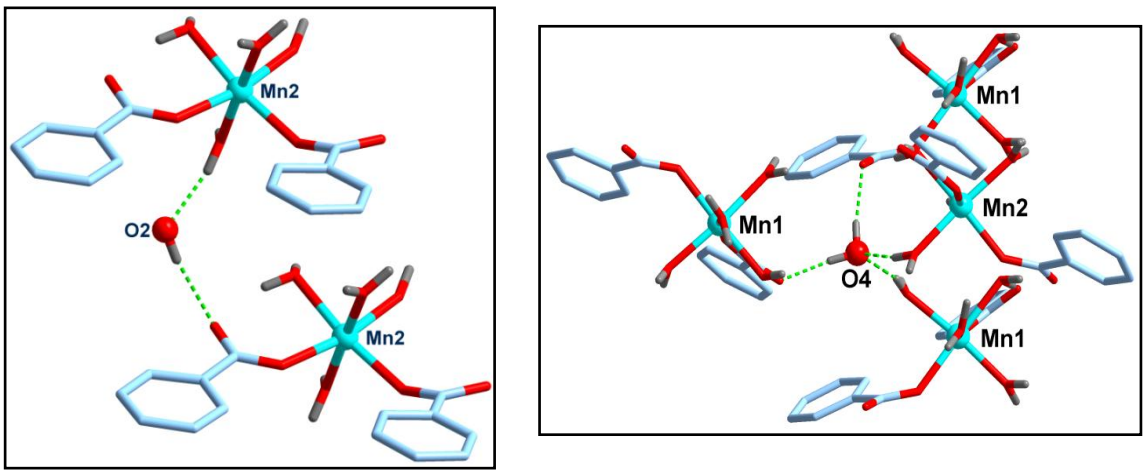

(**a**) (**b**)

Figure 3.19 Role of the lattice water molecules involving (**a**) O2 and (**b**) O4 oxygen atoms in stabilizing the supramolecular architectures of $[Mn(Bz)_2(H_2O)_4](4\text{-}CNpy)\cdot 2H_2O$ (**6**) via O–H···O hydrogen bonding interactions. Irrelevant aromatic H-atoms are omitted for clarity.

3.3.3.5 Theoretical study of compound $[Mn(Bz)_2(H_2O)_4](4\text{-}CNpy)\cdot 2H_2O$ (6)

To understand the nature of non-covalent interactions in the clathrate (inclusion) compound **6**, we have carried out topological analysis of electron density within the realm of quantum theory of atoms in molecules (QTAIM).[46] QTAIM provides unambiguous indication of the presence of various types of non-covalent interactions present in molecular aggregates by analyzing the presence of bond critical points and bond paths between the two atomic basins. QTAIM is based on those critical points where the gradient of the electron density, $\nabla\rho$, vanishes. Such points are classified by the curvature of the electron density. For example, a bond critical point has one positive curvature (along the inter-nuclear direction) and two negative curvatures (perpendicular to the bond). Two bonded atoms are then connected by a bond path through this bond critical point. The presence of such bond critical points is a universal indicator of interaction between the atoms.[86] Generally, for closed-shell interactions (such as ionic, van der Waals or hydrogen bonds), the electron density at bond critical points, ρ_b, is small (<0.01 a.u) and Laplacian, $\nabla^2\rho$, is positive.

Figure 3.20(a) shows the molecular graph of supramolecular tetramer of Mn(II) with enclathrated *4-CNpy* molecules involving various non-covalent interactions.

However, our major effort is focused on analyzing the C–H···C interaction owing to its unavailability in the published literature, although they were identified earlier, studied theoretically for a few modelled compounds and established crystallographically. It is evident from **Figure 3.20(a)** that there is a formation of bond critical point and its associated bond path between the hydrogen atom of one unit and the carbon atom of the aromatic ring of the other unit. The value of electron density, ρ_b at the C–H···C bond critical point is 0.009 a.u., while the Laplacian of electron density, $\nabla^2\rho$, is 0.032 a.u. All the topological features indicate the presence of the novel C–H···C interaction in **6**.

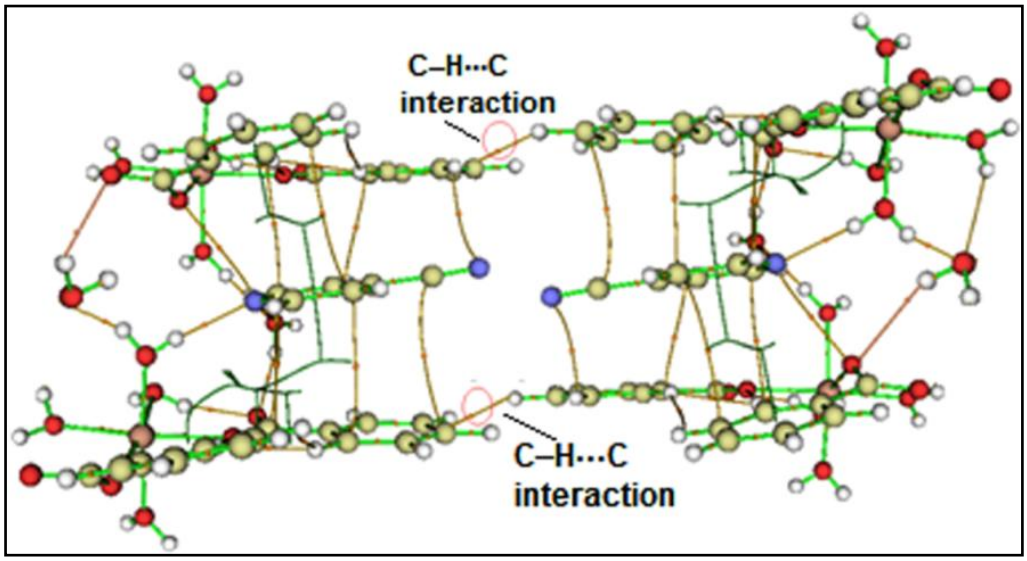

Figure 3.20(a) The molecular graph of supramolecular host tetramer of $[Mn(Bz)_2(H_2O)_4](4\text{-}CNpy)\cdot 2H_2O$ (**6**) with enclathrated *4-CNpy* molecules.

Non-covalent interaction (NCI) index, proposed by Yang and co-workers,[87] is one of the tools, which provide a qualitative mapping of the non-covalent interaction zone in real space. **Figure 3.20(b)** contains the non-covalent interaction (NCI) plot which clearly shows the presence of an attractive isosurface for C–H···C interaction in the supramolecular tetramer of **6**. These C–H···C interactions are capable enough to hold the two Mn(II) complex units together, suggesting their interaction energy should be significant. We therefore, calculated the interaction energy for these C–H···C interactions at M06-2X as well as B3LYP-D3BJ level of theory. B3LYP-D3BJ functional includes third generation of Grimme's empirical dispersion correction with

Beck-Johnson damping function.[88] The calculated interaction energies at M06-2X and B3LYP-D3BJ level of theory are –6.7 and –7.6 kcal/mol respectively. The calculated values of the interaction suggest that dispersion forces play an important role in these C–H···C interactions.

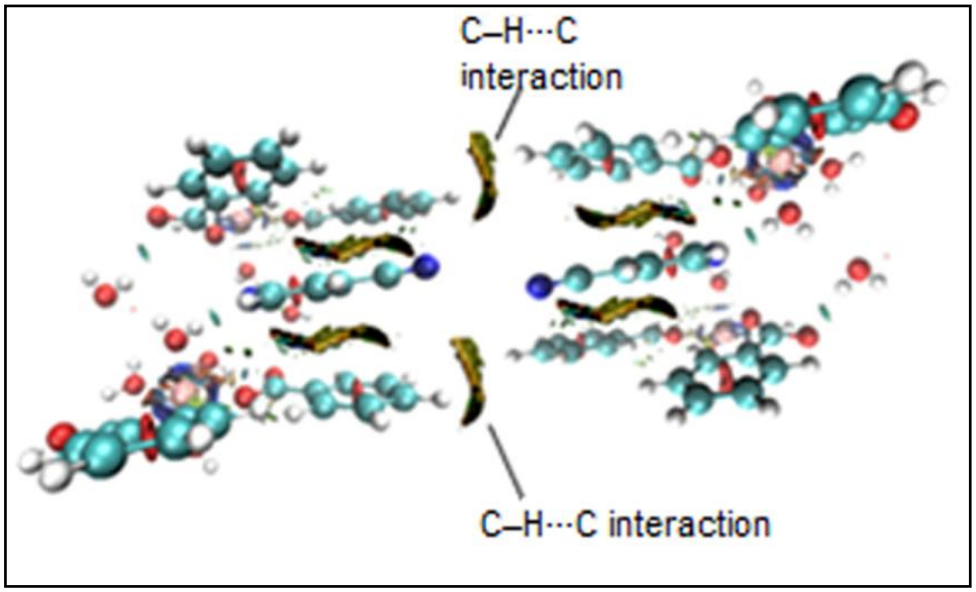

Figure 3.20(b) NCI plot of supramolecular host tetramer of $[Mn(Bz)_2(H_2O)_4](4\text{-}CNpy)\cdot 2H_2O$ (**6**) with enclathrated *4-CNpy* molecules.

We then further decomposed the energy into various physically meaningful components such as electrostatic, induction, dispersion and exchange using symmetry-adapted perturbation theory (SAPT). SAPT computes the non-covalent interaction energy directly without calculating the energies of individual components. Although various truncations of SAPT are available, we have used SAPT0 level of theory owing to the large size of the complex using PSI4 program.[89] **Table 3.7** contains the numerical data of SAPT0 analysis. It is clearly evident from **Table 3.7** that both electrostatics as well as dispersion interactions are the most dominant contributors towards the stabilization energy of the C–H···C interaction.

Table 3.7 SAPT0 analysis of the clathrate compound **6**. All energies are in kcal/mol.

Electrostatics	*Induction*	*Dispersion*	*Exchange*	*Total*
-4.42	-0.72	-4.13	5.21	-4.06

3.3.4 Thermal studies

Thermogravimetric analyses of complexes **4**, **5** and **6** were carried in 30-700°C under N_2 atmosphere at a heating rate of 10°C/min (**Figure 3.21**). For compound **4**, the 54.67% (calculated 55.8%) weight loss in the temperature range 35 to 264°C is due to the loss of two coordinated *4-NBz*.[90] V. Krishnakumar *et al*. have also reported the thermal decomposition of *4-NBz* in the similar temperature range in imidazolium 2-chloro-4-nitrobenzoate crystals.[91] In the temperature range 388 to 544°C, the weight loss of 34.50% (calculated 34.98%) corresponds to the loss of two *4-CNpy* moieties. Complex **5** undergoes thermal decomposition in two consecutive steps. The first two weight losses in the temperature range 155-257°C is due to the loss of the 1.5 *4-CNpy* molecules (observed weight loss 24.16%, calculated 23.06%).[92] S. Kapoor *et al*. have also reported decomposition of *4-CNpy* at 249°C in $[Ni(S_2COCH_2CH_2CH_3)_2(C_6H_4N_2)_2]$, [where, $C_6H_4N_2$ = 4-CNpy, $S_2COCH_2CH_2CH_3$ = O-propyldithiocarbonate].[93]

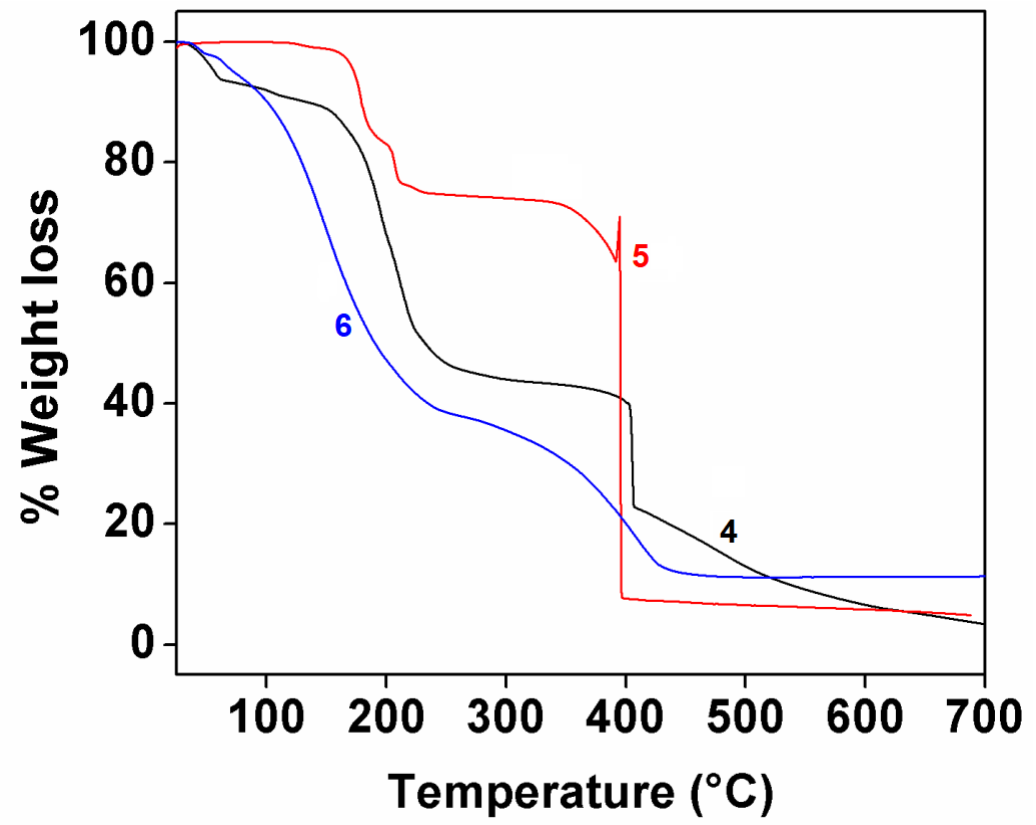

Figure 3.21 Thermogravimetric curves of compounds **4**, **5** and **6**.

The weight loss of 67.68% (calculated 68.76%) over the temperature range 339°C-628°C for complex **5** is caused by the loss of half of *4-CNpy* molecule and two molecules of *H_2BTC* moiety.[94] A. Majumder *et al*. have also reported the thermal decomposition of coordinated *H_2BTC* moiety above 380°C in $\{[Mn(H_2BTC)(phen)(H_2O)_2]H_2BTC.H_2O\}_n$ [where, H_3BTC = 1,3,5-benzene tricarboxylic acid, phen = phenanthroline].[95] For the inclusion compound **6**, the 2.09% (calculated 3.54%) weight loss up to 49°C is due to the removal of two lattice water molecules.[96] In the temperature range 59-274°C, the weight loss of 60.29% (calculated 62.00%) corresponds to the loss of remaining lattice and coordinated water molecules, two lattice *4-CNpy* molecules and two coordinated *Bz*. In the third stage of decomposition, weight loss of 24.77% (calculated 23.82%) in the temperature range of 287-700°C due to the loss of remaining two coordinated *Bz* moieties results in a decomposition product, MnO_2 (observed weight loss 11.18%, calculated 10.21%).[97] Thermogravimetric analyses of complexes **4**, **5** and **6** indicate that the complexes have considerable high thermal stability at room temperature.

3.4 CONCLUSIONS

Three new coordination complexes of Mn(II) *viz*. $[Mn(4\text{-}NBz)_2(4\text{-}CNpy)_2]_n$ (**4**), $[Mn(4\text{-}CNpy)_2(H_2BTC)_2]_n$ (**5**) and $[Mn(Bz)_2(H_2O)_4](4\text{-}CNpy)\cdot 2H_2O$ (**6**) have been synthesized and characterized by single crystal X-ray diffraction, electronic, vibrational spectroscopy and thermogravimetric analyses. The two polymers **4** and **5** are stabilized by several non-covalent interactions along with the rather unconventional nitrile-nitrile contacts resulting in layered assemblies. The supramolecular architectures in both the polymeric complexes also involve C–H···O interactions in a direction perpendicular to the existing layers that result in 3D network structures. We have evaluated the strength of the anti-parallel nitrile-nitrile interactions using DFT calculations which are enhanced by the coordination of *4-CNpy* to the Mn(II) metal centers. The interaction energy is similar to a H-bond (c.a. 5 kcal/mol for the water dimer) and consequently could be important in crystal engineering and supramolecular chemistry. In the clathrate compound **6**, however, the 2D architecture is stabilized by several non-covalent interactions *viz.* C–H···N, O–H···N, π–π and an unusual weak C–H···C contact. It is interesting to observe that the discrete monomer of **6** with enclathrated water and *4-*

CNpy results in a supramolecular host tetramer involving weak C–H···C contacts of significant energy. Both electrostatics as well as dispersion interactions are the most dominant contributors towards the stabilization of the unusual C–H···C contacts in compound **6**.

REFERENCES

1. (a) Wang, X.; Yao, W.; Qi, Y. F.; Luo, M. F.; Wang, Y. H.; Xie, H. W.; Yu, Y; Ma, R. Y.; Li, Y. G. *CrystEngComm.* **2011**, *13*, 2542.

(b) Zhu, Y. P.; Ma, T. Y.; Liu, Y. L.; Ren, T. Z.; Yuan, Z. Y. *Inorg. Chem. Front.* **2014**, *1*, 360.

(c) Lin, Q.; Fan, Y.; Mao, P.; Liu, L.; Liu, J.; Zhang, Y.; Yao, H.; Wei, T. *Eur. J. Chem*. **2018**, *24*, 777.

(d) Nangia, A. K.; Desiraju, G. R. *Angew. Chem. Int. Ed*. **2019**, *58*, 4100.

2. (a) Gu, J.; Wen, M.; Liang, X.; Shi, Z.; Kirillova, M. V.; Kirillov, A. M. *Cryst.* **2018**, *8*, 83.

(b) Nawrot, I.; Czerwińska, K.; Machura, B.; Kruszynski, R. *J. Lumin*. **2017**, *181*, 103.

(c) Ghosh, A. K.; Hazra, A.; Mondal, A.; Banerjee, P. *Inorg. Chim. Acta* **2019**, *488*, 86.

3. (a) Srinivasan, K.; Poornima, S.; Govindarajan, S.; Harrison, W. T. A. *J. Mol. Struct*. **2019**, *1184*, 519.

(b) Hu, H. L.; Suen, M. C.; Yeh, C. W.; Chen, J. D. *Polyhedron* **2005**, *24*, 1497.

(c) Jassal, A. K.; Sharma, S.; Hundal, G.; Hundal, M. S. *Cryst. Growth Des*. **2015**, *15*, 79.

(d) Wang, H.; Zhang, D.; Sun, D.; Chen, Y.; Zhang, L. F.; Tian, L.; Jiang, J.; Ni, Z. H. *Cryst. Growth Des*. **2009**, *9*, 5273.

4. (a) Wang, X. F.; Zhang, Y. B.; Huang, H.; Zhang, J. P.; Chen, X. M. *Cryst. Growth Des*. **2008**, *8*, 4559.

(b) Cheng, Q.; Qin, L.; Ke, C.; Zhou, J.; Lina, J.; Lin, X.; Zhang, G.; Cai, Y., *RSC Adv*. **2019**, *9*, 14750.

(c) Mikuriya, M.; Yoshioka, D.; Handab, M. *Coord. Chem. Rev*. **2006**, *250*, 2194.

(d) Boonmak, J.; Youngme, S.; Chaichit, N.; Albada, G. A. V.; Reedijk, J. *Cryst. Growth Des*. **2009**, *9*, 3318.

5. Veselska, O.; Cai, L.; Podbevsek, D.; Ledoux, G.; Guillou, N.; Pilet, G.; Fateeva, A., Demessence, A. *Inorg. Chem*. **2018**, *57*, 2736.

6. Miao, R.; Zhou, Q.; Wang, S.; Cheng, X.; Wang, D.; Huang, R. *J. Mol. Struct.* **2019**, *1184*, 219.

7. Li, C. H.; Zuo, J. L. *Adv. Mater*. **2020**, *32*, 1903762.

8. Xu, R., Xu, Y. *Modern Inorganic Synthetic Chemistry*, **2010**, Elsevier.

9. (a) Frontera, A., Ballester, P. *Aromatic Interactions: Frontiers in Knowledge and Application*, **2017**, *17*, 1.

(b) Feng, Z.; Zhang, T.; Wang, H; Xu, B.; *Chem. Soc. Rev*. **2017**, *46*, 6470.

(c) Politzer, P.; Murray, J. S.; Clark, T. *Phys. Chem.* **2013**, *15*, 11178

(d) Bauza, A.; Mooibroek, T. J.; Frontera, A. *Angew. Chem. Int. Ed*. **2013**, *52*, 12317.

(e) Mooibroek, T. J.; Gamez, P.; Reedijk, J. *CrystEngComm.* **2008**, *10*, 1501.

10. (a) Frontera, A.; Gamez, P.; Mascal, M.; Mooibroek, T. J.; Reedijk, J. *Angew. Chem. Int. Ed.* **2011**, *50*, 9564.

(b) Dutta, B.; Pratik, S. M.; Jana, S.; Sinha, C.; Datta, A.; Mir, M. H. *ChemistrySelect* **2018**, *3*, 4289.

(c) Maity, T.; Mandal, H.; Bauzá, A.; Samanta, B. C.; Frontera, A.; Seth, S. K. *New J. Chem*. **2018**, *42*, 10202.

(d) Brammer, L. *Faraday Discuss*. **2017**, *203*, 485.

(e) Caltagirone, C.; Gale, P. A. *Chem. Soc. Rev*. **2009**, *38*, 520.

11. Kim, D. S.; Kim, Y. S.; Guiver, M. D.; Pivovar, B. S. *J. Membrane Sci*. **2008**, *321*, 199.

12. Mueller-Westerhoff, U. T.; Nazzal, A.; Proessdorf, W. *J. Am. Chem. Soc*. **1981**, *103*, 7678.

13. Sharma, C. V. K; Broker, G. A.; Rogers, R. D. *J. Solid State Chem*. **2000**, *152*, 253.

14. Das, S.; Bharadwaj, P. K. *Inorg. Chem*. **2006**, *45*, 5257.

15. (a) Platts, J. A.; Howard, S. T.; Wozniak, K. *Chem. Commun*. **1996**, *1*, 63.

(b) Gronert, S.; Keeffe, J. R. *J. Am. Chem. Soc*. **2005**, *127*, 2324.

16. Ojala, C. R.; Ojala, W. H.; Britton, D. *J. Chem. Crystallogr*. **2011**, *41*, 464.

17. Lee, S.; Malik, A. B.; Fredrickson, D. C. *Cryst. Growth Des*. **2004**, *4*, 279.

18. Wood, P. A.; Borwick, S. J.; Watkin, D. J.; Motherwell, W. D. S.; Allen, F. H. *Acta Crystallogr*. **2008**, *64*, 393.

19. Desiraju, G. R.; Sharma, C. V. K. Crystal engineering and molecular recognition-twin facets of supramolecular chemistry. vol 2. Wiley, Chichester, **1996**.

20. (a) Yoon, M.; Srirambalaji, R.; Kim, K. *Chem. Rev*. **2012**, *112*, 1196.

(b) Okamura, T.; Wu, B.; Iguchi, H.; Breedlove, B. K.; Yamashita, M.; Kosaka, W.; Miyasaka, H.; Takaishi, S. *Chem. Commun*. **2017**, *53*, 6512.

(c) Wu, J.; Sun, X.; Guo, X.; Ji, M.; Wang, J.; Cheng, C.; Chen, L.; Wen, C.; Zhang, Q. *Food Biopro. Tech.* **2018**, *11*, 447.

21. Lee, J.; Kenney, J. W. *Solidification* **2018**, 72956.

22. (a) Kartal, Z.; Yavuz, A. *J. Mol. Struct*. **2018**, *1155*, 171.

(b) Khabibullin, A. R.; Huan, T. D.; Nolas, G. S.; Woods, L. M. *Acta Mater*. **2017**. *131*, 475.

(c) Wang, J.; Dolyniuk, J.; Kovni, K. *Acc. Chem. Res*. **2018**, *51*, 31.

23. Ni, Z. P.; Liu, J. L.; Hoque, M. N.; Liu, W.; Li, J. Y.; Chen, Y. C.; Tong, M. L. *Coord. Chem. Rev.* **2017**, *335*, 28.

24. (a) Li, Q.; Sha, X.; Li, S.; Wang, K.; Quan, Z.; Meng, Y.; Zou, B. *J. Phys. Chem. Lett.* **2017**, *8*, 2745.

(b) Murphy, M. J.; Zenere, K. A.; Ragon, F.; Southon, P. D.; Kepert, C. J.; Neville, S. M. *J. Am. Chem. Soc.* **2017**, *139*, 1330.

25. (a) Noa, F. M. A.; Bourne, S. A.; Su, H.; Nassimbeni, L. R. *Cryst. Growth Des*. **2017**, *17*, 1876.

(b) Peraka, K. S.; Lusi, M.; Bajpai, A.; Zaworotko, M. J. *Cryst. Growth Des*. **2017**, *17*, 959.

(c) Saha, U.; Dutta, D.; Bauzá, A.; Frontera, A.; Sarma, B.; Bhattacharyya, M. K. *Polyhedron* **2019**, *159*, 387.

26. Wicht, M. M.; Su, H.; Báthori, N. B.; Nassimbeni, L. R. *CrystEngComm*. **2016**, *18*, 2509.

27. Valverde-Muñoz, F. J.; Bartual-Murgui, C.; Piñeiro-López, L.; Muñoz, M. C.; Real, J. A. *Inorg. Chem.* **2019**, *58*, 10038.

28. Vishweshwar, P.; McMahon, J. A.; Peterson, M. L.; Hickey, M. B.; Shattock, T. R.; Zaworotko, M. J. *Chem. Commun*. **2005**, *17*, 4601.

29. Sokolov, A. N.; Friscic, T.; MacGillivray, L. R. *J. Am. Chem. Soc*. **2006**, *128*, 2806.

30. Friscic, T.; MacGillivray, L. R. *Chem. Commun*. **2005**, 5748.

31. Karki, S.; Friscic, T.; Jones, W.; Motherwel, W. D. S. Mol. Pharm. **2006**, *4*, 347.

32. McNamara, D. P.; Childs, S. L.; Giordano, J.; Iarriccio, A.; Cassidy, J.; Shet, M. S.; Mannion, R.; O'Donnel, E.; Park, A. *Pharm. Res*. **2006**, *23*, 1888.

33. Nehm, S. J.; Rodriguez-Spong, B.; Rodriguez-Hornedo, N. *Cryst. Growth Des*. **2006**, *6*, 592.

34. (a) Bollaa, G.; Nangia, A. *Chem. Commun*. **2016**, *52*, 5748.

(b) Gadade, D. D.; Pekamwar, S. S. *Adv. Pharm. Bull*. **2016**, *6*, 479.

35. SADABS, V2.05, Bruker AXS, Madison, USA, **1999**.

36. Brandenburg, K. Diamond 3.1f, Crystal Impact GbR, Bonn, Germany, **2008**.

37. Gaussian 09, Revision C.01, Frisch, M. J.; Trucks, G. W.; Schlegel, H. B.; Scuseria, G.; Robb, M. A.; Cheeseman, J. R.; Scalmani, G.; Barone, V.; Petersson, G. A.; Nakatsuji, H.; Li, X.; Caricato, M.; Marenich, A.; Bloino, J.; Janesko, B. G.; Gomperts, R.; Mennucci, B.; Hratchian, H. P.; Ortiz, J. V.; Izmaylov, A. F.; Sonnenberg, J. L.; Williams-Young, D.; Ding, F.; Lipparini, F.; Egidi, F.; Goings, J.; Peng, B.; Petrone, A.; Henderson, T.; Ranasinghe, D.; Zakrzewski, V. G.; Gao, J.; Rega, N.; Zheng, G.; Liang, W.; Hada, M.; Ehara, M.; Toyota, K.; Fukuda, R.; Hasegawa, J.; Ishida, M.; Nakajima, T.; Honda, Y.; Kitao, O.; Nakai, H.; Vreven, T.; Throssell, K.; Montgomery Jr,. J. A.; Peralta, J. E.; Ogliaro, F.; Bearpark, M.; Heyd, J. J.; Brothers, E.; Kudin, K. N.; Staroverov, V. N.; Keith, T.; Kobayashi, R.; Normand, J.; Raghavachari, K.; Rendell, A.; Burant, J. C.; Iyengar, S. S.; Tomasi, J.; Cossi, M.; Millam, J. M.; Klene, M.; Adamo, C.; Cammi, R.; Ochterski, J. W.; Martin, R. L.; Morokuma, K.; Farkas, O.; Foresman, J. B.; Fox, D. J. Gaussian, Inc., Wallingford CT, **2016**.

38. Zhao, Y.; Truhlar, D. G. *Theor. Chem. Acc*. **2008**, *120*, 215.

39. (a) Sadhukhan, D.; Maiti, M.; Pilet, G.; Bauzá, A.; Frontera, A.; Mitra, S. *Eur. J. Inorg. Chem.* **2015**, *11*, 1958.

(b) Mirzaei, M; Eshtiagh-Hosseini, H.; Bolouri, Z.; Rahmati, Z.; Esmaeilzadeh, A.; Hassanpoor, A.; Bauza, A.; Ballester, P.; Barceló-Oliver, M.; Mague, J. T.; Notash, B.; Frontera, A. *Cryst. Growth Des.* **2015**, *15*, 1351.

(c) Chakraborty, P.; Purkait, S.; Mondal, S.; Bauzá, A.; Frontera, A.; Massera, C.; Das, D. *CrystEngComm.* **2015**, *17*, 4680.

40. Boys, S. B.; Bernardi, F. *Mol. Phys*. **1970**, *19*, 553.

41. Spartan'10, Wavefunction Inc. Irvine, CA.

42. Bader, R. F. W. *Chem. Rev.* **1991**, *91*, 893.

43. AIMAll (Version 17.11.14), Keith, T. A., Gristmill, T. K. Software, Overland Park KS, USA, **2017** (aim.tkgristmill.com)

44. Zhao, Y.; Truhlar, D. G. *Theor. Chem. Acc.* **2008**, *120*, 215.

45. Dolg, M.; Wedig, U.; Stoll, H.; Preuss, H. *J. Chem. Phys*. **1987**, *86*, 866.

46. (a) Bader, R. F. W., Atoms in Molecules: A Quantum Theory, Oxford Univ. Press, Oxford, **1990**.

(b) Bader, R. F. W. *J. Phys. Chem. A*. **1998**, *102*, 7314.

(c) Zhao, Y.; Truhlar, D. G. *J. Chem. Phys*. **2006**, *124*, 194101.

47. Tian, L. M. *A Multifunctional Wavefunction Analyzer* (version 3.1). Available from: http://Multiwfn.codeplex.com. Accessed May 22, **2015**.

48. Gaussian 16, Revision A.03, Frisch, M. J.; Trucks, G. W.; Schlegel, H. B.; Scuseria, G. E.; Robb, M. A.; Cheeseman, J. R.; Scalmani, G.; Barone, V.; Petersson, G. A.; Nakatsuji, H.; Li X.; Caricato, M.; Marenich, A. V.; Bloino, J.; Janesko, B. G.; Gomperts, R.; Mennucci, B.; Hratchian, H. P.; Ortiz, J. V.; Izmaylov, A. F.; Williams-Young, J. L.; Ding, F.; Lipparini, F.; Egidi, F.; Goings, J.; Peng, B.; Petrone, A.; Henderson, T.; Ranasinghe, D.; Zakrzewski, V. G.; Gao, J.; Rega, N.; Zheng, G.; Liang W.; Hada, M.; Ehara, M.; Toyota, K.; Fukuda, R.; Hasegawa, J.; Ishida, M.; Nakajima, T.; Honda, Y.; Kitao, O.; Nakai, H.; Vreven, T.; Throssell, K.; Montgomery Jr., J. A.; Peralta, J. E.; Ogliaro, F.; Bearpark, M. J.; Heyd, J. J.; Brothers, E. N.; Kudin, K. N.; Staroverov, V. N.; Keith, T. A.; Kobayashi, R.; Normand, J.; Raghavachari, K.; Rendell, A. P.; Burant, J. C.; Iyengar, S. S.; Tomasi, J.; Cossi, M.; Millam, J. M.; Klene, M.; Adamo, C.; Cammi, R.; Ochterski, J. W.; Martin, R. L.; Morokuma, K.; Farkas, O.; Foresman, J. B.; Fox, D. J. Gaussian, Inc., Wallingford C. T. **2016**.

49. Wang, G.; Yin, J.; Li, J.; Yin, Z.; Zhang, W.; Xi, Z. *Inorg. Chem. Front*. **2019**, *6*, 428.

50. Lu, J. F.; Qiao, L. J.;. Li, L. Q; Liu, Z. H. *J. Mol. Struct*. **2015**, *1081*, 79.

51. Massoud, S. S.; Broussard, K. T.; Mautner, F. A.; Vicente, R.; Saha, M. K.; Bernal, I. *Inorg. Chim. Acta* **2008**, *361*, 123.

52. Xu, Y.; Ding, F.; Liu, D.; Yang, P.; Zhu, L. *J. Mol. Struct*. **2018**, *1155*, 72.

53. Iqbal, M.; Ali, S.; Tahir, M. N. *J. Struct. Chem*. **2018**, *59*, 1619.

54. (a) Zhao, H.; Bodach, A.; Heine, M.; Krysiak, Y.; Glinnemann, J.; Alig, E.; Fink, L.; Schmidt, M. *CrystEngComm.* **2017**, *19*, 2216.

(b) Sharma, P.; Gogoi, A.; Verma, A. K.; Frontera, A.; Bhattacharyya, M. K. *New J. Chem*. **2020**, *44*, 5473.

(c) Dutta, D.; Islam, S. M. N.; Saha, U.; Chetry, S.; Guha, A. K.; Bhattacharyya, M. K. *J. Mol. Struct*. **2019**, *1195*, 733.

55. Kumar, C. S. C.; Panicker, C. Y.; Fun, H. K; Mary, Y. S.; Harikumar, B.; Chandraju, S.; Quah, C. K.; Ooi, C. W. *Spectrochim. Acta A.* **2014**, *126*, 208.

56. Wu, G.; Shi, X.; Fang, Q.; Tian, G.; Wang, L.; Zhu, G.; Addison, A. W.; Wei, Y.; Qiu, S.; *Inorg. Chem. Commun*. **2003**, *6*, 402.

57. Tahli, A.; Koc, U.;. Elshaarawy, R. F. M; Kautz, A. C.; Janiak, C.; *Cryst*. **2016**, *6*, 23.

58. Masoudiasl, A.; Montazerozohori, M.; Joohari, S.; Taghizadeh, L.; Mahmoudi, G.; Assoud, A. *Ultrason. Sonochem*. **2019**, *52*, 244.

59. Shi, Z.; Li, G.; Wang, L.; Gao, L.; Chen, X.; Hua, J.; Feng, S. *Cryst. Growth Des*. **2004**, *4*, 25.

60. Jin, J., Han, X.; Meng, Q.; Li, D.; Chi, X. Y.; Niu, S. Y. *J. Solid State Chem*. **2013**, *197*, 92.

61. (a) Bhattacharyya, M. K.; Devi, P. G.; Dasgupta, D.; Bora, S. J.; Das, B. K. *Polyhedron* **2012**, *35*, 62.

(b) Ghosh, M.; Majee, A.; Nethaji, M.; Chattopadhyay, T. *Inorg. Chim. Acta* **2009**, *362*, 2052.

62. Zheng, Y.; Li, X.; Li, Y.; Wu, Z.; Yan, C. *J. Photochem. Photobiol*. **2012**, *114*, 27.

63. Kar, P.; Drew, M. G. B.; Gomez-Garcia, C. J.; Ghosh, A. *Polyhedron* **2013**, *50*, 229.

64. Ye, R.; Zhang, X.; Qin, Y.; Yao, Y. *CrystEngComm*. **2017**, *19*, 1658.

65. Srinivasan, B. R; Rane, G. K. *J. Chem. Sci*. **2009**, *121*, 145.

66. Srinivasan, B. R; Tari, S. P; Parsekar, N. U; Narvekar, K. U. *Indian J. Chem*. **2020**, *59*, 51.

67. (a) Das, B. K.; Bora, S. J.; Bhattacharyya, M. K.; Barman, R. K. *Acta Cryst. B* **2009**, *65*, 467.

(b) Islam, S. M. N.; Dutta, D.; Frontera, A.; Bhattacharyya, M. K. *Inorg. Chim. Acta* **2019**, *487*, 424.

68. Desiraju, G. R.; Steiner, T. The Weak Hydrogen Bond in Structural Chemistry and Biology; Oxford University Press: Oxford, U.K. **1999**.

69. Panja, A.; Shaikh, N.; Vojtı, P.; Gao, S.; Banerjee, P. *New J. Chem*. **2002**, *26*, 1025.

70. Liu, S.; Cao, C.; Yang, F.; Yu, M.; Yao, S.; Zheng, T.; He, W.; Zhao, H.; Hu, T.; Bu, X. *Cryst. Growth Des*. **2016**, *16*, 6776.

71. Nemec, I.; Herchel, R.; Trravnicek, Z. *Dalton Trans*. **2018**, *47*, 1614.

72. Sakiyama, H.; Ichi, M.; Mitsuhashi, R.; Mikuriya, M. *X-Ray Struct. Anal. Online* **2017**, *33*, 29.

73. Zhu, C.; Wang, Y.; Mao, Q.; Li, F.; Li, Y.; Chen, C. *Materials* **2017**, *10*, 313.

74. Nasr, M. B.; Kahlaoui, M.; Ferenc, W.; Cristovao, B.; Nasr, C. B. *J. Struct. Chem*. **2018**, *59*, 1317.

75. Badar, R. F. W. *J. Phys. Chem. A* **1998**, *102*, 7314.

76. Sadhukhan, D.; Maiti, M.; Pilet, G.; Bauzá, A.; Frontera, A.; Mitra, S. *Eur. J. Inorg. Chem.* **2015**, *33*, 1958.

77. (a) Kar, P.; Drew, M. G. B.; Gomez-Garcia, C. J.; Ghosh, A. *Polyhedron* **2013**, *50*, 229.

(b) Nastase, S.; Tuna, F.; Maxim, C.; Muryn, C. A.; Avarvari, N.; Winpenny, R. E. P.; Andruh, M. *Cryst. Growth Des*. **2007**, *7*, 1825.

78. Hwang, I. H.; Jo, Y. D.; Kim, H. Y.; Kang, J.; Noh, J. Y.; Hyun, M. Y.; Kim, C.; Kim, Y.; Kim, S. J. *Polyhedron* **2012**, *42*, 282.

79. Cui, G.; He, C.; Jiao, C.; Geng, J.; Blatov, V. A. *CrystEngComm*. **2012**, *14*, 4210.

80. Gogoi, A.; Saha, U.; Dutta, D.; Bhattacharyya, M. K. *J. Struct. Chem*. **2019**, *60*, 324.

81. Chakravorty, S.; Platts, J. A; Das, B. K. *Dalton Trans*. **2011**, *40*, 11605.

82. Sun, D.; Wei, Z.; Yang, C.; Wang, D.; Zhang, N.; Huang, R.; Zheng, L. *CrystEngComm*. **2011**, *13*, 1591.

83. Sreejith, S. S.; Mohan, N.; Kurup, M. R. P. *Polyhedron* **2017**, *135*, 278.

84. Das, S.; Bharadwaj, P. K. *Inorg. Chem.* **2006**, *45*, 5257.

85. Nasri, S.; Amiri, N.; Turowska-Tyrk, I.; Daranc, J.; Nasri, H. *Acta Cryst. E* **2016**, *72*, 164.

86. (a) Bader, R. F. W. *Chem. Rev*. **1991**, *91*, 893.

(b) Zhao, Y; Truhlar, D. G. *J. Chem. Phys*. **2006**, *124*, 194101.

87. Contreras-Garcia, J.; Johnson, E. R.; Keinan, S.; Chaudret, R.; Piquemal, J. P.; Beratan, D. N.; Yang, W. *J. Chem. Theory Comput*. **2011**, *7*, 625.

88. (a) Becke, A. D. *J. Chem. Phys*. **1993**, *98*, 5648.

(b) Lee, C.; Yang, W.; Parr, R. G. *Phys. Rev. B* **1988**, *37*, 785.

(c) Vosko, S. H.; Wilk, L.; Nusair, M. *Can. J. Phys*. **1980**, *58*, 1200.

(d) Becke, A. D.; Johnson, E. R. *J. Chem. Phys*. **2005**, *123*, 154101.

(e) Johnson, E. R.; Becke, A. D. *J. Chem. Phys*. **2005**, *123*, 024101.

(g) Stephens, P. J.; Devlin, F. J.; Chabalowski, C. F.; Frisch, M. J. *J. Phys. Chem*. **1994**, *98*, 11623.

89. Turney, J. M.; Simmonett, A. C.; Parrish, R. M.; Hohenstein, E. G.; Evangelista, F. A.; Fermann, J. T.; Mintz, B. J.; Burns, L. A.; Wilke, J. J.; Abrams, M. L.; Russ, N. J.; Leininger, M. L.; Janssen, C. L.; Seidl, E. T.; Allen, W. D.; Schaefer, H. F.; King, R. A.; Valeev, E. F.; Sherrill, C. D.; Crawford, T. D. *WIREs Comput. Mol. Sci*. **2012**, *2*, 556.

90. Bala, R.; Kaur, A.; Kashyap, M.; Janzen, D. E. *J. Mol. Struct*. **2014**, *1063*, 203.

91. Krishnakumara, V.; Jayaprakash, J.; Boobas, S.; Komathi, M. *Eur. Phys. J*. **2016**, *131*, 375.

92. Islam, S. M. N.; Dutta, D.; Guha, A. K.; Bhattacharyya, M. K. *J. Mol. Struct*. **2019**, *1175*, 130.

93. Kapoor, S.; Sachar, R.; Singh, K.; Gupta, V. K.; Rajnikant, *J. Chem. Crystallogr*. **2012**, *42*, 458.

94. Ying, S. M.; Mao, J. G. *Eur. J. Inorg. Chem*. **2004** 1270.

95. Majumder, A.; Shit, S.; Choudhury, C. R.; Batten, S. R.; Pilet, G.; Luneau, D.; Daro, N.; Sutter, J.; Chattopadhyay, N.; Mitra, S. *Inorg. Chim. Acta* **2005**, *358*, 3855.

96. Huang, W.; Hu, D.; Gou, S.; Qian, H.; Fun, H. K.; Raj, S. S. S.; Meng, Q. *J. Mol. Struct.* **2003**, *649*, 269.

97. (a) Hwang, I. H.; Jo, Y. D.; Kim, H. Y.; Kang, J.; Noh, J. Y.; Hyun, M. Y.; Kim, C.; Kim, Y.; Kim, S. J. *Polyhedron* **2012**, *42*, 282.

(b) Sun, D.; Wei, Z. H.; Yang, C. F.; Wang, D. F.; Zhang, N.; Huang, R. B.; Zheng, L. S. *CrystEngComm*. **2011**, *3*, 1591.